Carbohydrate Polymers 344 (2024) 122519

Contents lists available at ScienceDirect

Carbohydrate Polymers

journal homepage: www.elsevier.com/locate/carbpol

Surface modification of cellulose nanomaterials with amine functionalized fluorinated ionic liquids for hydrophobicity and high thermal stability

Onajite T. Abafe Diejomaoh [a], Alessandra Lavoratti [a], Jude Laverock [b], Todor T. Koev [c], Yaroslav Z. Khimyak [c], Tetsuo Kondo [d], Stephen J. Eichhorn [a,*]

[a] Bristol Composites Institute, School of Civil, Aerospace and Design Engineering, University of Bristol, University Walk, Bristol BS8 1TR, UK
[b] School of Chemistry, University of Bristol, Bristol BS8 1TS, UK
[c] School of Pharmacy, University of East Anglia, Norwich Research Park, NR4 7TJ, UK
[d] Institute of Agriculture, Tokyo University of Agriculture and Technology, Fuchu, Tokyo 183-8538, Japan

ARTICLE INFO

Keywords:
Fluorinated ionic liquids
Cellulose nanocrystals
Cellulose nanofibers
Surface modification
Hydrophobization

ABSTRACT

A highly hydrophobic fluorinated ionic liquid (IL), 3-aminopropyl-tributylphosphonium bis(trifluoromethylsolfonyl)imide ([aP_{4443}][NTf_2]), was synthesized, and applied for the surface modification of cellulose nanomaterials (CNMs) by reductive amination. The modified CNMs were fully characterized for their chemical structure, morphology, thermal stability, and surface hydrophobicity. Results obtained from Nuclear Magnetic Resonance spectroscopy (^{1}H, ^{13}C, ^{19}F and ^{31}P), Fourier Transform Infrared spectroscopy, X-ray Photoelectron Spectroscopy, and X-ray diffraction confirmed the successful grafting of [aP_{4443}][NTf_2] onto the surface of CNMs up to a degree of surface functionalization of 2.5 %. Transmission Electron Microscopy analysis confirmed the dimensions of the CNMs were retained after modification but with significant aggregation for modified cellulose nanocrystals (CNCs). Thermal Gravimetric Analysis demonstrated significant increases in the degradation temperatures of modified CNCs from ~252 °C to ~310 °C. Modified cellulose nanofibers (CNFs) did not show any increase in thermal stability. The modified CNM suspensions showed reduced affinity for water and the formation of aggregates in aqueous media. Furthermore, a water contact angle test demonstrated enhanced hydrophobicity for modified CNMs. This modification approach holds potential for the use of the [aP_{4443}][NTf_2] IL for functional materials to achieve novel hydrophobic CNMs suitable for aqueous processing with thermoplastics, for fabrication of thermally stable composite materials, and for polymer gel electrolytes for batteries.

1. Introduction

Current global issues such as dwindling oil reserves, carbon emissions, plastic pollution, and sustainability have led to a need to accelerate research efforts towards seeking alternatives to fossil-fuels in the development of new materials. Cellulose, which is an abundant biopolymer produced at a rate of 10^{11} - 10^{12} t yr^{-1} in nature (Klemm et al., 2005; Nechyporchuk et al., 2016), presents a sustainable resource, and has an extensive range of applications in the production of biomedical materials, supercapacitors, batteries, catalytic supports, paper, cosmetics, textiles, food coatings, packaging materials, barrier/separation membranes, cements, explosives etc. (Eichhorn et al., 2022; Habibi, 2014; Lyne, 2013; Robert J Moon et al., 2016). Nano-sized cellulose materials (1–100 nm), which have been extensively investigated in this respect, vary in dimensions, properties, and composition depending on the production conditions. They can be found in a variety of forms, including cellulose nanocrystals (CNCs) and cellulose nanofibres (CNFs) (Eichhorn et al., 2022). These materials possess several appealing qualities such as high mechanical strengths (2–6 GPa) (Saito et al., 2013) and stiffnesses (143 GPa) (Šturcová et al., 2005), and a high surface to volume ratio because of their typically narrow transverse dimensions. Their high axial stiffness, along the chain, has often been thought to be mainly due to the presence of three prominent surface hydroxy groups in each anhydro glucose unit (AGU) capable of forming strong intra and intermolecular hydrogen bonds networks (Eichhorn et al., 2022). The influence of hydrogen bonding has however sometimes been overstated, and other interactions, such as van der Waals, also play a significant role (Wohlert et al., 2022). The presence of these hydroxy groups along the cellulose chains however gives cellulose nanomaterials (CNMs) a natural affinity with water and can hinder its interaction with

* Corresponding author.
E-mail address: s.j.eichhorn@bristol.ac.uk (S.J. Eichhorn).

https://doi.org/10.1016/j.carbpol.2024.122519
Received 28 March 2024; Received in revised form 16 July 2024; Accepted 17 July 2024
Available online 20 July 2024

hydrophobic polymers (Etale et al., 2023; Wohlert et al., 2022). This hydrophilic nature to cellulose nanomaterials could also be detrimental in applications where water absorption deters the material application, such as in the transportation of liquids and gases in nano cellulose materials and in nano papers that are often used in food packaging (Bideau et al., 2018).

The hydrophilicity of cellulose can be reduced by attaching hydrophobic groups to the reactive hydroxy groups, a process known as the "hydrophobization of cellulose", which can be achieved by either chemical modification or physical adsorption pathways. While the physical adsorption pathways result in reversible products, chemical modification is most preferred due to the formation of the products by covalent bonds with hydroxy groups on the CNM surface (Nigmatullin et al., 2020). For this purpose, only mild reaction conditions, with controlled reaction times, are recommended to avoid complete alteration to the cellulose structure. A variety of chemical modification routes to facilitate the interaction of CNMs with polymers in aqueous media have been developed over the past decades. Some of these routes have involved the formation of esters and carbamates on the CNM surfaces (Cellante et al., 2018; Y. Wang et al., 2018), grafting of polymers through ring opening polymerization (Majoinen et al., 2011), acylation (Casarano & El Seoud, 2013), silanization (Beaumont et al., 2018), etherification with tosyl chlorides (Gericke et al., 2012) and the most relevant to the present work being the grafting of amine to carbonyl groups formed from the periodate oxidation of the glucose ring (Dash et al., 2012). This latter route to modification is of particular interest as amines are versatile compounds with reactive nitrogen, which are capable of introducing other functionalities to polymer composites (Froidevaux et al., 2016).

We have recently explored the reductive amination of CNCs with alkyl amines (8 and 16 carbon chain lengths), finding that the introduction of these groups results in uniquely hydrophobized materials (Nigmatullin et al., 2020). This uniqueness demonstrates an affinity for hydrophobic materials, but since the modification is light, they also interact with water – making a so-called "amphiphilic cellulose" (Onyianta et al., 2022). These materials have been demonstrated to interact with polypropylene in aqueous media, subsequently forming polypropylene-CNC composites with enhanced properties (Onyianta et al., 2022). An overview of the many routes to the hydrophobization of CNMs has indicated that most chemical surface modification processes are either complex or associated with the use and release of toxic substances. However, owing to the fact that sustainability and green chemistry are two main directional factors for the next generation of polymer composites materials, the use of ionic liquids for surface modification of CNMs has been proposed as a sustainable solution to this issue (Casarano & El Seoud, 2013; Gericke et al., 2012; Yahia et al., 2019).

Ionic liquids (IL), which are low melting salts (<100 °C), comprise an asymmetric organic cation and an organic or inorganic anion. They have been demonstrated to play significant roles in chemical reactions (Casarano & El Seoud, 2013; Gericke et al., 2012; Wasserscheid & Welton, 2008; Thomas Welton, 1999). This ability is due to their high thermal stability and their considerably lower vapour pressure compared to conventional organic solvents. They are normally referred to as environmentally-benign and "green solvents" (Thomas Welton, 1999; T. Welton, 2011). The application of ILs encompasses a wide range of chemical reactions extending to the dissolution of cellulose in the range 18–24 wt%, having significant impacts in the development of high modulus fibres (Zhu et al., 2016; Zhu et al., 2018). These unique solvents are key for the production of CNMs, and can be prepared from $>10^{12}$ ion combinations and several functional groups, giving them the name "designer solvents" (Plechkova & Seddon, 2007). Frequently employed IL systems comprise cations such as imidazolium, pyrrolidinium, pyridinium, triazolium and ammonium ions paired with halide, carboxylic $[RCO_2]^-$ or fluorinated anions such as tetrafluoroborate ($[BF_4]^-$), hexafluorophosphate ($[PF_6]^-$), or bis(trifluoromethylsulfonyl) imide ($[NTf_2]^-$ or TFSI) (Abafe Diejomaoh et al., 2023; Wasserscheid & Welton, 2008; Yahia et al., 2019).

The phosphonium cation, which holds a lot of potential for use in ILs, is less expensive to prepare, less toxic and more thermally stable when compared to imidazolium or nitrogen based ionic liquids. These cations have larger sizes, higher polarizability, and lower binding energy with anions (Macarie et al., 2019) compared to other forms. Furthermore, they are efficient reagents and catalysts for use in mild green reactions (Macarie et al., 2019). The phosphonium ionic liquids have displayed good potential in various reactions including the functionalization of proteins, where phosphonium chlorides have been employed to successfully modify lysozymes (Camplo et al., 2011). As it is with other cations, the efficiency of phosphonium cations in chemical applications depends on the choice of the substituents on the phosphorus atom and anionic part. Generally, ionic liquids can be rendered hydrophobic by incorporating either the cation or anion with a long alkyl chain or a fluorinated anion respectively (Fukumoto & Ohno, 2006). In the present work, a highly hydrophobic ionic liquid 3-aminopropyl-tributylphosphonium bis(trifluoromethylsulfonyl)imide ($[aP_{4443}][NTf_2]$) was synthesized, and employed to achieve surface modification of CNCs and CNFs. The choice of the bis(trifluoromethylsulfonyl)imide (CF_3SO_2-N-SO_2CF_3) anion commonly referred to as $[NTf_2]^-$ was based on its hydrophobic nature, which is due to the high electronegativity of fluorine atoms, with low electron density and net negative charge on the anion structure resulting in enhanced hydrophobic properties (~ 1000 ppm in equilibrium with liquid water) (Earle et al., 2006; Ullah et al., 2019). Additionally, the $[NTf_2]^-$ based ionic liquids possess a high thermal stability [18] with thermal decomposition temperatures of most $[NTf_2]^-$-based ILs; values up to 400 °C. Furthermore, the unique feature of the strong C—F bonds present in fluorinated $[NTf_2]^-$-based ionic liquids can contribute to the rigidity, dispersion properties, ionic conductivity and electrochemical stability of the modified CNMs (Salam et al., 2015). This type of ionic liquid has recently been integrated with polymers in electrochemical applications such as in gel polymer electrolytes as flexible supercapacitors (Jamil & Silvester, 2022; Pilathottathil et al., 2018; X. Wang et al., 2017) and also as flame retardants to reduce the flammability of composites (Khazalpour et al., 2020; Sonnier et al., 2016).

Ionic liquids are green solvents which can be designed to possess hydrophobic properties potentially offering sustainable solutions to the hydrophilicity of CNMs. To demonstrate this concept, a hydrophobic ionic liquid namely, 3-aminopropyl-tributylphosphonium bis(trifluoromethylsulfonyl)imide ($[aP_{4443}][NTf_2]$), was designed and applied in various amounts for surface modification of CNMs by reductive amination of oxidized CNMs. This approach resulted in a moderately hydrophobized and thermally stable CNMs. Our hypothesis is that in only mildly modifying the surface we might be able to retain the water interactions of the material as well, retaining some aqueous processing capability.

Furthermore, we would like to emphasize that the IL ($[aP_{4443}][NTf_2]$) employed in this work is composed of a phosphonium cation and a bis(trifluoromethylsulfonyl)imide anion which by virtue does not only give it a high thermal stability and hydrophobicity but also flame retardancy and high ionic conductivity. Surface modification of CNMs with this ionic liquid is very promising for sustainable practices and broadens the applicability of CNMs as coatings for packaging papers, textiles, and furniture, as well as its use for polymer gel electrolytes to improve safety in lithium ion batteries.

2. Experimental session

2.1. Materials

Sodium-form sulfated (sCNCs) (11.5 wt%) were supplied by the University of Maine. Based on the dimensions of the CNCs (see Section 3.3) the average molecular weight (MW) was calculated as 7858 g

mol^{-1}. CNFs (0.003 wt%), obtained by aqueous counter collision (Kondo et al., 2014) of Bamboo Kraft Pulp (Degree of Polymerization = 7.6×10^2, MW 123,120 g mol^{-1}, from Chuetsu Pulp & Paper Company, Ltd., Toyama, Japan), at the Tokyo University of Agriculture and Technology. 3-bromopropylamine hydrobromide (98 %), tributylphosphine (≥93.5 %), lithium bis(trifluoromethyl)sulfonyl imide, sodium periodate, sodium chloride, sodium cyanoborohydride, isopropyl alcohol, hexane, acetonitrile, dimethyl sulfoxide (DMSO), and Dowex ion-exchange resin were supplied by Sigma Aldrich/Merck (Dorset, United Kingdom). Ultrapure water was used for all experiments. The 3-aminopropyl-tributylphosphonium bis(trifluoromethylsulfonyl) imide ($[aP_{4443}][NTf_2]$) ionic liquid, sCNCs and CNFs investigated herein were prepared in our laboratory using previously established procedures.

2.2. Synthesis of amine functionalized fluorinated ionic liquid

The synthesis of an amine functionalized fluorinated ionic liquid known as 3-aminopropyl-tributylphosphonium bis(trifluoromethylsulfonyl)imide ($[aP_{4443}][NTf_2]$) followed a two-step reaction process; quaternization to obtain 3-aminopropyl-tributylphosphonium bromide hydrobromide ($[aP_{4443}][Br].[HBr]$) and anion exchange reaction to $[aP_{4443}][NTf_2]$. The synthesis procedure is illustrated in Scheme 1. The syntheses of similar compounds have been previously reported (Bradaric et al., 2003; Khazalpour et al., 2020; Liu & Sie, 2016; Macarie et al., 2019; Ullah et al., 2019; Yue et al., 2022). However, to the best of our knowledge this is the first report on the synthesis of 3-aminopropyl-tributylphosphonium bis(trifluoromethylsulfonyl)imide ($[aP_{4443}][NTf_2]$), and certainly its use to modify CNMs.

2.2.1. Quaternization reaction to obtain 3-aminopropyl-tributylphosphonium bromide hydrobromide

3-aminopropyl-tributylphosphonium bromide hydrobromide ($[aP_{4443}][Br].[HBr]$) was prepared by reacting a mixture of tri-n-butylphosphine (9.24 g, 0.046 mol) and 3-bromopropylamine hydrobromide (10 g, 0.046 mol) in acetonitrile (20 mL) contained in a round bottom flask, fitted with a rotary condenser. The mixture was heated to 80 °C with vigorous stirring for 48 h. On completion, acetonitrile was evaporated under reduced pressure at 80 °C and the residue was dried under vacuum at 80 °C for 24 h with a Schlenk line. The product was washed with hexane under reflux for 1 h and dried at 80 °C for 24 h with a Schlenk line to yield a white solid of $[aP_{4443}][Br]{\cdot}HBr$ in 70 % yield (by mass).

2.2.2. Anion exchange to obtain 3-aminopropyl-tributylphosphonium bis(trifluoromethylsulfonyl) imide

3-aminopropyl-tributylphosphonium bromide hydrobromide ($[aP_{4443}][Br].[HBr]$) (6.30 g, 0.015 mol) and lithium bis(trifluoromethylsulfonyl) imide $LiNTf_2$ (6.37 g, 0.02 mol) were each dissolved in distilled (10 mL) water and poured into a round bottom flask. The mixture was stirred at room temperature for 24 h then left to stand for phase separation comprising an organic ionic liquid and an aqueous phase. The IL phase was separated and then extracted eight times with 20 mL portions of deionised water, to remove any impurities. During each extraction step, small samples of the aqueous phase were collected and tested for residual chloride by the addition of a drop of 0.10 M $AgNO_3$, followed by observation for precipitate until none was detected. The formed IL was dried on a rotary evaporator for 4 h at a temperature and pressure of 40 °C and 72 mbar, respectively. Further drying of the product under vacuum while stirring at 60 °C for an additional 8 h gave a pale yellow coloured 3-aminopropyl-tributylphosphonium bis(trifluoromethylsulfonyl)imide ($[aP_{4443}][NTf_2]$) at an 85 % yield (by mass).

2.3. Surface modification of CNMs

The surface modification reactions of CNMs with the IL ($[aP_{4443}][NTf_2]$) followed a procedure from previous reports (Dash et al., 2012; Nigmatullin et al., 2020; Onyianta et al., 2022) and was achieved by their oxidation using sodium periodate, followed by a reductive amination. Details of the reaction are described below and presented in Scheme 2.

2.3.1. Oxidation of CNMs

An aqueous suspension of sulfated cellulose nanocrystals (sCNCs) (2.5 wt%) or cellulose nanofibres (CNFs) (0.3 wt%) was added to a beaker and dispersed using sonication (operating at a 10 % amplitude for 2 min). Following this, 1.68 mmol of sodium periodate to 1 g of CNM was added to the mixture. The mixture was wrapped in foil to prevent photoinduced decomposition of sodium periodate and stirred at room temperature for 24 h. Thereafter, the reaction with the CNCs was quenched with ethylene glycol. This quenching step was subsequently

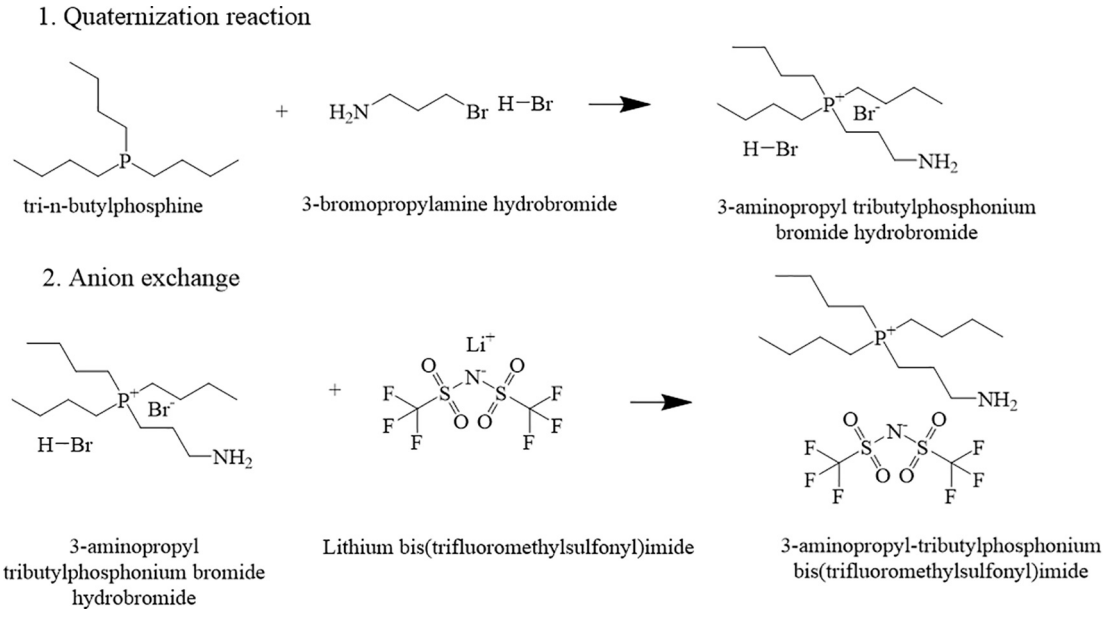

Scheme 1. Reaction mechanism for the synthesis of 3-aminopropyl-tributylphosphonium bis(trifluoromethylsulfonyl)imide ($[aP_{4443}][NTf_2]$).

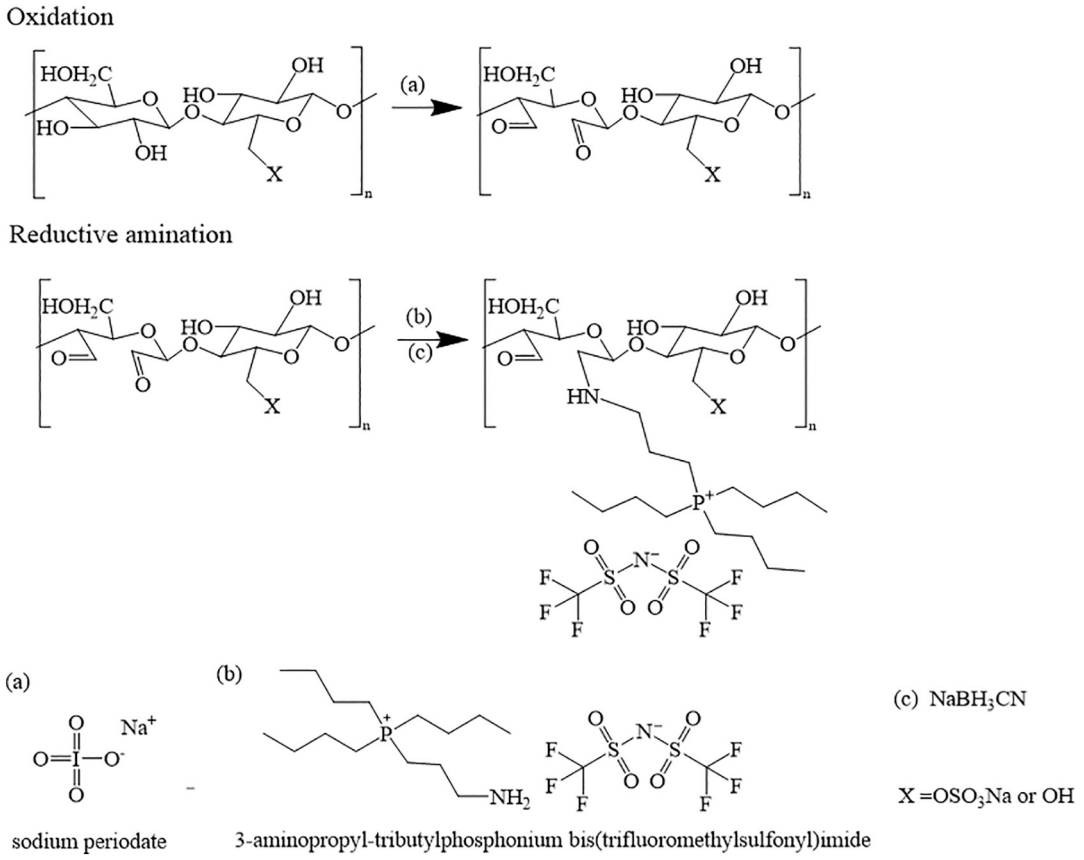

Scheme 2. Synthetic steps leading to the formation of ionic liquid modified CNMs (where X is OSO_3Na^- for CNCs or OH for CNFs).

omitted for the oxidation of the CNFs due to the possibility of side reactions from ethylene glycol that has been recently reported (Simon et al., 2023). The CNFs are thought to be more susceptible to the prevalence of side reactions, which are normally observed with an excess of periodate (Simon et al., 2023). Since we are only performing a mild reaction it is thought that this would be negligible, but it is acknowledged that ethylene glycol can be avoided in the washing steps. Oxidized CNMs with dialdehyde groups were purified by precipitating with NaCl (2 wt%) solution and using repeated centrifugation to isolate the dialdehyde CNCs (DACNC) or dialdehyde CNFs (DACNF) which was redispersed in deionised water and further purified by dialysis in dialysis tubes having a molecular weight cut-off of 6–8 kD for 24 h.

2.3.2. Reductive amination of dialdehyde CNMs with [aP_{4443}][NTf_2]

An aqueous suspension of DACNC was added to beakers containing appropriate amounts of [aP_{4443}][NTf_2] required to obtain mixtures with concentrations of 1 wt%, 3 wt%, 10 wt%, 20 wt% and 50 wt% [aP_{4443}][NTf_2] in DACNC. The mixtures were then heated individually to 45 °C and stirred at 350 rpm for 3 h with a magnetic stirrer equipped with a thermostat after which the solutions were allowed to cool to ambient temperature. Consequently, sodium cyanoborohydride (2.5 % equivalent of [aP_{4443}][NTf_2]) was added to each mixture and stirred for a further 21 h at room temperature. The amination reaction was stopped by adding an excess of 2-propanol, followed by three centrifugation and washing cycles at 10,000 rpm for 5 min each. The recovered modified CNCs were then redispersed in deionised water using an ultra turrax disperser operating at 10,000 rpm for 1 min and further purified by dialysing against distilled water for at least 3 days, with frequent changes of the water. The procedure was repeated with an aqueous suspension of DACNF to obtain 10 wt% [aP_{4443}][NTf_2] in CNF and also to obtain a blank containing 10 wt% [aP_{4443}][NTf_2] in CNC without the addition of sodium cyanoborohydride.

2.4. Characterization of CNMs

The unmodified and modified CNMs were analysed with various techniques for their chemical and surface structure, morphology, water interactions, and thermal stabilities.

2.4.1. Fourier transform infrared (FTIR) spectroscopy

Changes to the chemical functionalities of the CNMs resulting from the modification process were analysed using a Spectrum 100 spectrometer (Perkin-Elmer, USA) equipped with a diamond crystal ATR tip. The samples were air dried and placed directly on the diamond crystal and spectra were taken within a wavenumber region of 4000 to 400 cm^{-1} with 16 scans at a resolution of 4 cm^{-1}. ATR correction on the spectra was performed by fitting the transmittance from 0 to 100 using Origin software.

2.4.2. Solution-state nuclear magnetic resonance (NMR) analysis

Nuclear magnetic resonance (NMR) measurements for the [aP_{4443}][NTf_2] were performed on a Jeol ECZ 400 NMR spectrometer at a frequency of 400 MHz for ^1H NMR and 100 MHz for ^{13}C NMR. The [aP_{4443}][NTf_2] was dissolved in deuterated dimethyl sulfoxide (DMSO-d_6) and its resonance at 2.50 ppm was used as internal reference for ^1H NMR.

Modified CNCs (10 wt% IL-CNC) were dissolved in DMSO-d_6 (ca. 10 mg/mL). ^1H-^{13}C heteronuclear multiple bond correlation (HMBC) spectra were recorded at 20 °C, using 16 scans, a recycle delay of 1 s, and a 84 ms long-range coupling evolution period.

2.4.3. Solid-state NMR analysis

^1H-^{13}C Cross-Polarization Magic Angle Spinning (CP/MAS) NMR experiments were performed on a Bruker Avance III NMR spectrometer, equipped with a 4-mm triple resonance probe operating at frequencies of 300.13 MHz (^1H) and 75.48 MHz (^{13}C). The ionic liquid was pipetted

directly into a 4-mm rotor insert sealed with a stopper and a cap, whereas the powder materials were packed directly into an 80-μL rotor, and spun at a MAS rate of 10 kHz. All ^{1}H-^{13}C CP/MAS NMR spectra were acquired at 20 °C using a minimum of 6 k scans, a recycle delay of 10 s, and a contact time of 2 ms. ^{19}F direct detection experiments were acquired with a minimum of 256 scans and a relaxation delay of 10 s. Spectral deconvolution was performed via a global spectral deconvolution (GSD) algorithm using the MestreLab MNova (v14.2) software package.

2.4.4. X-ray photoelectron spectroscopy (XPS)

XPS analysis was performed with a Scienta Omicron Argus analyzer, with an emission angle of 35° and a monochromatic Al Kα source (1486.7 eV) operating at 15 kV and 18 mA (270 W). Prior to the measurements, well-dispersed aqueous suspensions of unmodified and modified CNMs were drop casted onto Mo substrates, and allowed to dry. They were then mounted onto a Ta backplate with carbon tapes. Thereafter, they were loaded into an ultra-high vacuum chamber within 90 min to outgas for 3 days before measurement. All samples were charged under X-ray illumination and required charge neutralisation. The charge neutraliser was set to 4 μA of the beam current with a beam energy of 6 eV. Spectra were acquired at the start and end of each sample illumination to check for X-ray beam induced modifications. Survey spectra were recorded with a pass energy of 50 eV and high-resolution spectra were recorded with a pass energy of 20 eV.

2.4.5. X-ray diffraction analysis

X-ray diffraction (XRD) patterns were obtained from freeze dried CNMs with a Bruker D8 Advance powder X-ray Diffractometer using Cu radiation (λ = 1.541 Å) and a PSD LynxEye detector. The samples were measured while spinning at a rate of 1 s/step, and using a 2θ step size of 0.02°. XRD data were obtained in the range of 2θ = 5–50°. Background measurements were performed prior to scanning the CNM samples and the degree of crystallinity (crystallinity index) of each sample was calculated from background subtracted data according to the peak area method using the equation (Salem et al., 2023)

$$CI(\%) = \frac{A_{cr}}{A_{sample}} \times 100\% \quad (1)$$

where $CI(\%)$ is the percentage crystallinity index, A_{cr} is the area of all the crystalline peaks, A_{sample} is the total area of all the diffraction space.

2.4.6. Transmission electron microscopy (TEM)

Transmission electron microscopy (TEM) was employed to investigate possible changes to the morphologies of the CNMs resulting from surface modification. The unmodified and modified CNM suspensions (0.001 wt%) were sonicated at a 10 % amplitude for 10 min and casted onto freshly glow-discharged carbon-coated copper grids. To ensure a true representation of the sample in solution, a washing step was performed to remove the effect of casting. Thereafter, the samples were negatively stained with aqueous 2 wt% uranyl acetate before drying and imaging. Images were obtained by a 200 kV field-emission gun transmission electron microscope (JEM-2100F, from JEOL, Japan), equipped with an Orius SC1000 camera, from Gatan (now AMETEK), USA.

2.4.7. Determination of surface charge density of sCNCs

Surface charge densities of modified and unmodified CNCs were determined via the titration of aqueous suspensions containing 0.05 g dry weight of material against a 10 mM NaOH solution while measuring the change in the conductivity. The titration procedure was adapted from a method reported in the literature (Abitbol et al., 2013; Beck et al., 2015). Prior to titration, 0.6 g of Dowex Marathon C hydrogen form strong acid cation exchange resin (corresponding to 12 g resin to 1 g of CNC) was added to the suspension and stirred at room temperature for 1 h. After this, the resin was separated from the solution by decantation. This step was carried out to ensure full protonation of the surface moieties of the CNCs. Subsequently, 1 mL of 100 mM NaCl solution was added to increase the conductivity response and the solution made up to 100 mL before titration. The molar surface charge of CNCs was determined graphically by plotting the corrected conductivity of the suspension as a function of the volume of NaOH added. The equivalence point which is the volume of the titrant was obtained from the plot as the intersection point of the linear regressions of the regions before and after the first equivalence point and the mean value was used to determine the surface charge on the CNCs from the sulfate half-ester group. The total surface charge density X was calculated as mmol kg^{-1} of CNC using the equation

$$X = \frac{C_{NaOH} * V_{NaOH}}{m_{CNC}} \quad (2)$$

where C_{NaOH} is the concentration of the titrant (NaOH) in mmol/L, V_{NaOH} is the volume of titrant at the equivalence point in litres, and m_{CNC} is the dry mass of the CNCs.

2.4.8. Zeta potential analysis

CNM suspensions were diluted to 1 mg ml^{-1} (w/v) using deionised water. Zeta potential measurements comprising 20 runs were performed in triplicate using a Zetasizer Nano-ZS (Malvern, UK) with a DTS 1070 capillary cell at the refractive index of water (n = 1.33) and at 25 °C.

2.4.9. Water contact angle measurement

Water contact angle (WCA) measurements were carried out by first preparing thin films of 1 wt% and 0.5 wt% CNCs and CNFs suspensions respectively at ambient temperature by spin coating. Subsequently, contact angles were obtained using a sessile drop with a DSA100 Drop Shape Analyzer (KRÜSS) equipped with a calibrated ultra-thin needle. Several drops of deionised water (2 μL per drop) were made on each film and digital images of their contact angles were recorded every 0.5 s for 30 s. Thereafter, average values of three drops with their standard deviations were obtained.

2.5. Thermal gravimetry analysis (TGA)

The thermal degradation properties of the CNMs was investigated by TGA (Netasch, STA 449F3). Approximately 5 mg of each sample were analysed in an alumina pan. All tests were performed under a nitrogen atmosphere with a gas flow of 10 mL/min and heated from 40 to 800 °C at a heating rate of 10 °C/min.

3. Results and discussion

3.1. Surface modification of CNMs with $[aP_{4443}][NTf_2]$

In an attempt to introduce hydrophobic properties to the CNMs they were modified by first creating a dialdehyde linkages on the 2nd and 3rd carbon positions by oxidation with periodate. The oxidation reaction was followed by grafting dialdehyde CNMs with 3-aminopropyltributylphosphonium bis(trifluoromethylsulfonyl)imide ($[aP_{4443}][NTf_2]$) by reductive amination.

For the purpose of the reductive amination reaction, a hydrophobic ionic liquid appended with a primary amine functionality is required. The $[NTf_2]^-$-based ionic liquids are known to possess hydrophobic properties so 3-aminopropyl-tributylphosphonium bis(trifluoromethylsulfonyl)imide ($[aP_{4443}][NTf_2]$) was synthesized via a two-step process involving the quaternization reaction from commercially available tri-n-butylphosphine and 3-bromopropylamine hydrobromide to obtain 3-aminopropyl tributylphosphonium bromide hydrobromide $[aP_{4443}][HBr][Br]$ followed by anion exchange of $[aP_{4443}][HBr][Br]$ with lithium bis(trifluoromethylsulfonyl)imide ($LiNTf_2$) to obtain the desired anion. NMR and FTIR spectroscopies were employed to confirm

the chemical structure of $[aP_{4443}][NTf_2]$. The ^{1}H NMR and FTIR spectra are presented in Figs. 1 and 2 respectively while ^{13}C NMR spectra, NMR chemical shift assignments and wavenumbers are presented in Supplementary information. As shown in the ^{1}H NMR spectra in Fig. 1, the peaks obtained are numbered and correspond to the different protons contained in the tributyl and aminopropyl chains linked to the phosphonium cation of $[aP_{4443}][NTf_2]$. The ^{13}C spectra indicated signals with chemical shifts corresponding to the carbon atoms present in the $[aP_{4443}][NTf_2]$ (Supplementary information). Furthermore, FTIR spectra of $[aP_{4443}][NTf_2]$ (Fig. 2) showed distinctive signals, such as a broad absorption at ~3183 cm^{-1} from N—H groups, C—H stretching at 2900 cm^{-1}, P—C in the region of 789 cm^{-1}, and C—N at 1187 cm^{-1}, which could be attributed to the cation while distinct signals of S═O at 1342 cm^{-1} are characteristic of the $[NTf_2]^-$ anion and correlate with similar reported ionic liquids (Pringle et al., 2003) confirming the success of the synthesis.

Subsequently, various concentrations of $[aP_{4443}][NTf_2]$ was grafted to the CNMs. Modified CNCs containing 1 wt%, 3 wt%, 10 wt%, 20 wt% and 50 wt%, of $[aP_{4443}][NTf_2]$ referred to as 1 wt% IL-CNC, 3 wt% IL-CNC, 10 wt% IL-CNC, 20 wt% IL-CNC and 50 wt% IL-CNC respectively were prepared by a reductive amination reaction of the $[aP_{4443}][NTf_2]$ with DACNC. A blank 10 wt% IL-CNC was also prepared without the reductive amination step (i.e, without the addition of sodium cyanoborohydride). Subsequently, 10 wt% of $[aP_{4443}][NTf_2]$ in CNF, referred to as 10 wt% IL-CNF was prepared from a reductive amination reaction of the $[aP_{4443}][NTf_2]$ with DACNF. While the full range of modified CNCs and 10 wt% IL-CNFs was employed to determine the degree of surface functionalization, only modified 3 wt% IL-CNC and 10 wt% IL-CNC as well as 10 wt% IL-CNFs were chosen for detailed characterization compared to their respective unmodified forms. The reason for choosing these concentrations was to avoid the formation of excessive aggregated structures and to enable relationships to be drawn within the properties of a stable suspension.

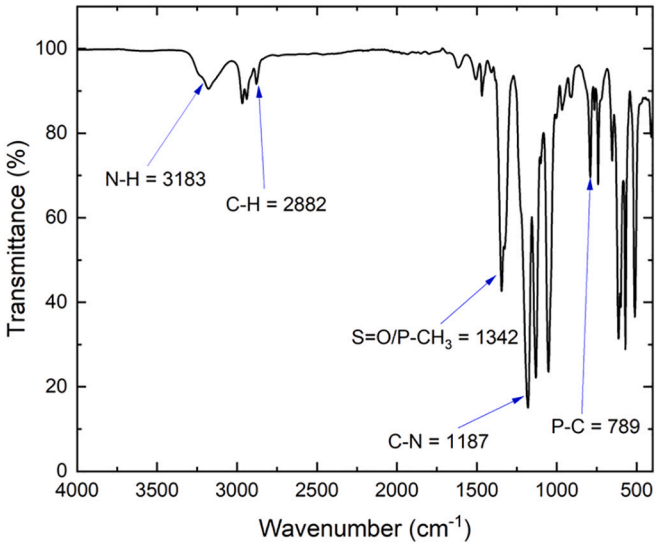

Fig. 2. A typical FT-IR spectrum of 3-aminopropyltributylphosphonium bis (trifluoromethylsulfonyl) imide $[aP_{4443}][NTf_2]$.

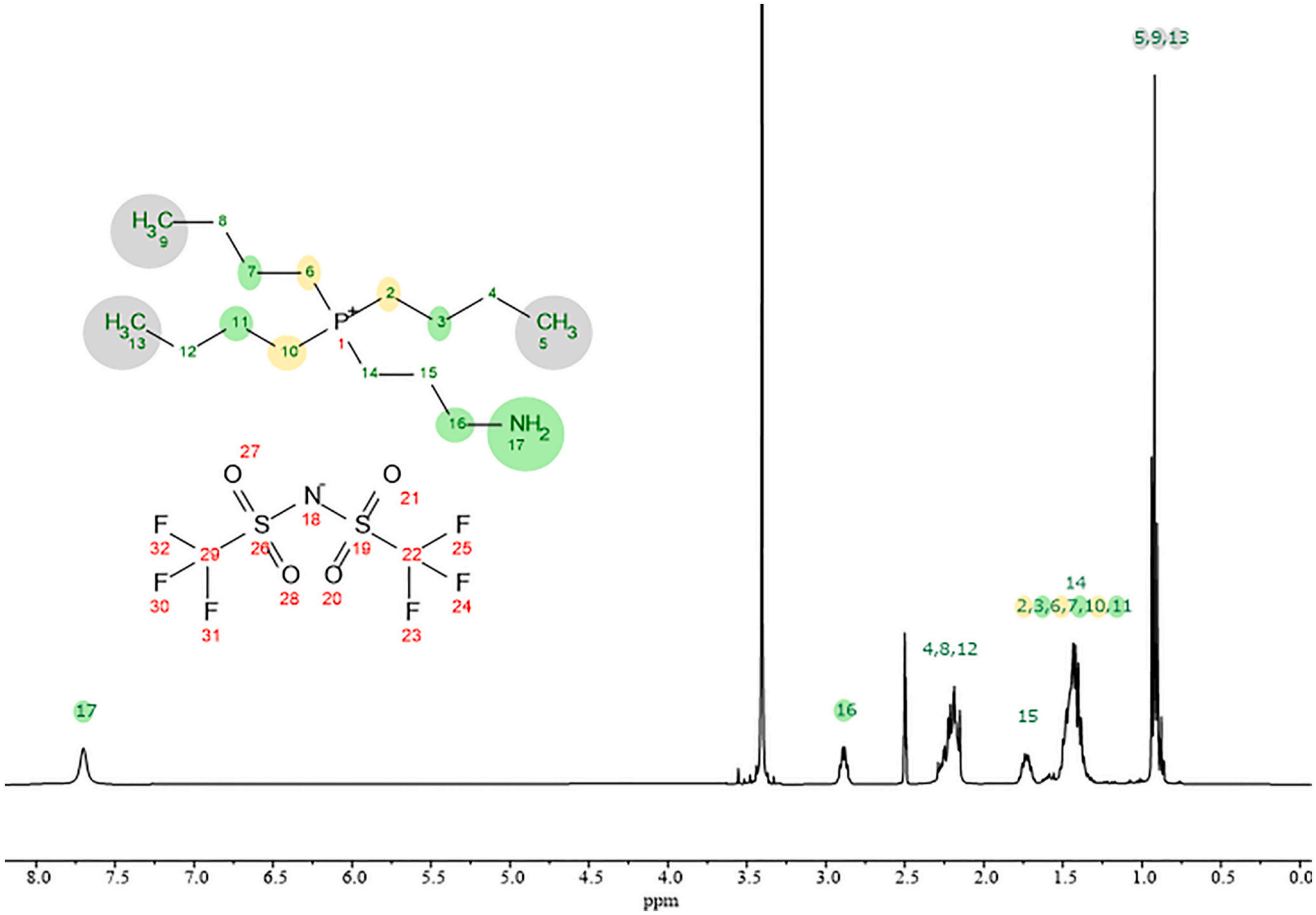

Fig. 1. A typical H NMR spectrum of 3-aminopropyltributylphosphonium bis (trifluoromethylsulfonyl) imide ($[aP_{4443}][NTf_2]$) in DMSO-d_6.

3.2. Chemical structure analysis of CNMs

3.2.1. Fourier transform infrared (FTIR) spectroscopy

FTIR analysis was applied to investigate the functionalization of the CNMs. The spectra obtained are compared in Figs. 3a&b. The spectra from modified and unmodified CNCs showed strong and broad absorption bands located at ~3350 cm^{-1}, which have been attributed to inter and intramolecular hydrogen bonds. An absorption band located at ~2894 cm^{-1} is attributed to C—H stretching, and was clearly visible in all spectra (Alila et al., 2009). The bands observed in the region of 1630–900 cm^{-1} in all spectra are typical of cellulose; namely bands located at ~1428, 1367, 1334, 1027 cm^{-1} and 896 cm^{-1} due to stretching and bending vibrations of -CH_2 and -CH, -OH and C—O bonds respectively (Onyianta et al., 2022; Xu et al., 2013). The band located at ~1730 cm^{-1}, observed in the DACNC spectrum, is attributed to a C═O stretch from the aldehyde groups, confirming the oxidation of the CNCs prior to grafting with the $[aP_{4443}][NTf_2]$ (Dash et al., 2012).

Bands relating to functional groups such as N—H, C—N and S═O at wavenumber positions of ~1650, 1187 and 1342 respectively, which were expected to be present in the modified CNCs from the grafting processes of DACNC with the $[aP_{4443}][NTf_2]$, were not observed in the 3 wt% and 10 wt% IL-CNC spectra. This was probably due to the low concentration of the $[aP_{4443}][NTf_2]$ as well as an overlapping of other functional groups in this region. Analysing the spectra for unmodified and modified CNFs, showed absorbances similar to the CNCs as outlined above, and typical of cellulose (Lu et al., 2008; Qu et al., 2012). No changes were observed in the spectra of 10 wt% IL-CNFs making them insufficient in confirming the success of the modification.

3.2.2. ^{13}C CP-MAS and ^{19}F NMR analyses

^{1}H-^{13}C CP/MAS spectra shown in Fig. 4a exhibited typical cellulose peaks for the CNCs (Onyianta et al., 2022; G. Xu et al., 2024) with additional peaks in the 10–30 ppm range, assigned to the carbon sites (CH_3/CH_2) from the cation moiety in $[aP_{4443}][NTf_2]$, suggesting the presence of $[aP_{4443}][NTf_2]$ on the CNCs' surfaces. Surprisingly, carbon signals from CF_3 in the $[NTf_2]^-$ anion of $[aP_{4443}][NTf_2]$, which is expected to be present in the modified CNMs, were not detected. Therefore, to further confirm the presence of $[aP_{4443}][NTf_2]$ on the surface of the modified CNMs, a ^{19}F direct detection NMR experiment was performed. A ^{19}F peak at ca. -76.1 ppm (Fig. 5) was present in both the solid- and solution-state ^{19}F NMR spectra of the 10 wt% CNC and solid-state ^{19}F NMR spectra of $[aP_{4443}][NTf_2]$, confirming the presence of the $[NTf_2]^-$ moiety in the modified CNCs. In addition, the ^{19}F solid-state NMR spectrum of 10 wt% IL-CNC (Fig. 5) exhibits a shoulder peak at −78.5 ppm, suggesting more than one type of ^{19}F-containing functionalisation that could be from ionically interacting or physically adsorbed fluorine in a peak ratio of 1:0.36. However, discriminating between which peak corresponds to a specific mode of binding was not performed in this study. Further verification with ^{1}H-^{13}C HMBC spectrum of 10 wt % IL-CNC (Fig. S2) showed the presence of a crosspeak at ca. 4.51 ppm (^{1}H)/31.5 ppm (^{13}C) revealing the presence of a long-range covalent bond between CNC and $[aP_{4443}][NTf_2]$ thus confirming a successful

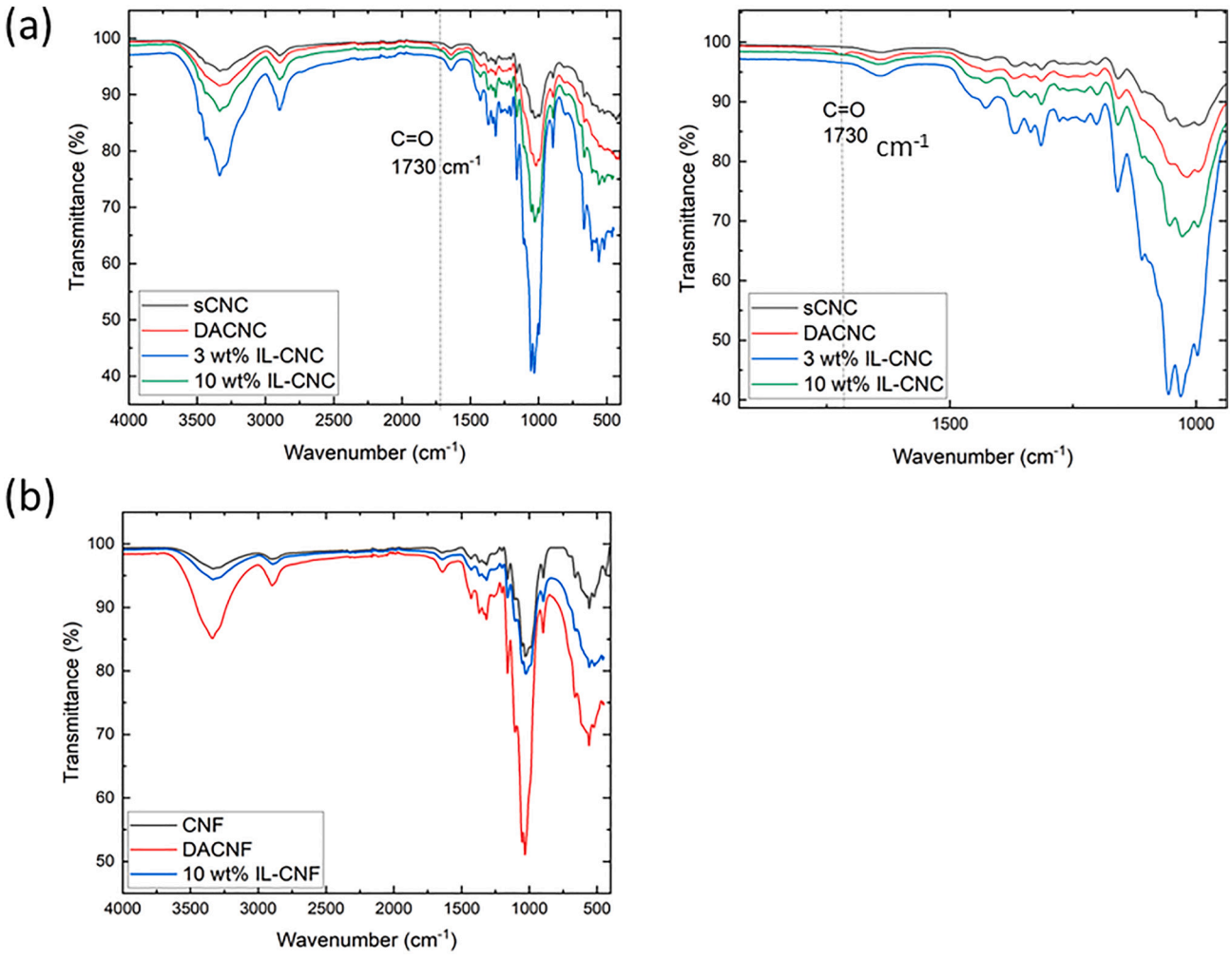

Fig. 3. FT-IR spectra comparison for the (a) IL modified and unmodified CNCs (The spectral region showing −C=O stretching from the aldehyde groups is magnified on the right), and (b) IL modified and unmodified CNFs.

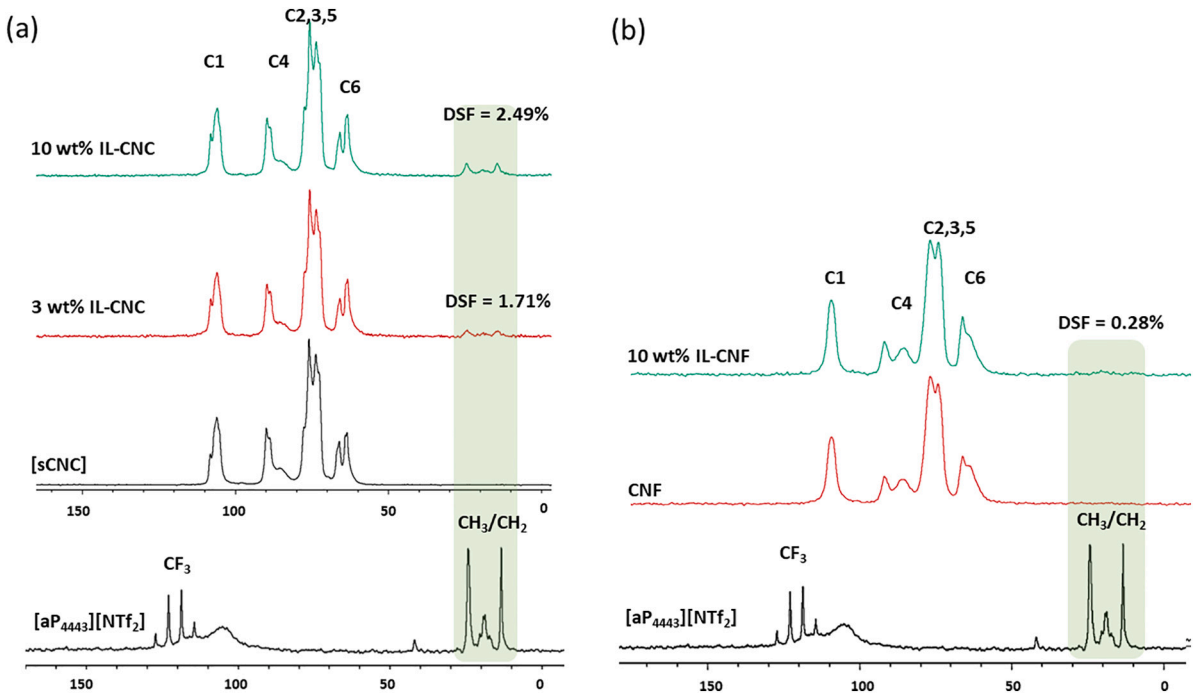

Fig. 4. ^{1}H-^{13}C CP/MAS NMR spectral overlay of (a) $[aP_{4443}][NTf_2]$ with sCNC, 3 wt% IL-CNC and 10 wt% IL-CNC (b) $[aP_{4443}][NTf_2]$ with CNF and 10 wt% IL-CNF. (Highlighted region shows presence of the tributyl cation from $[aP_{4443}][NTf_2]$).

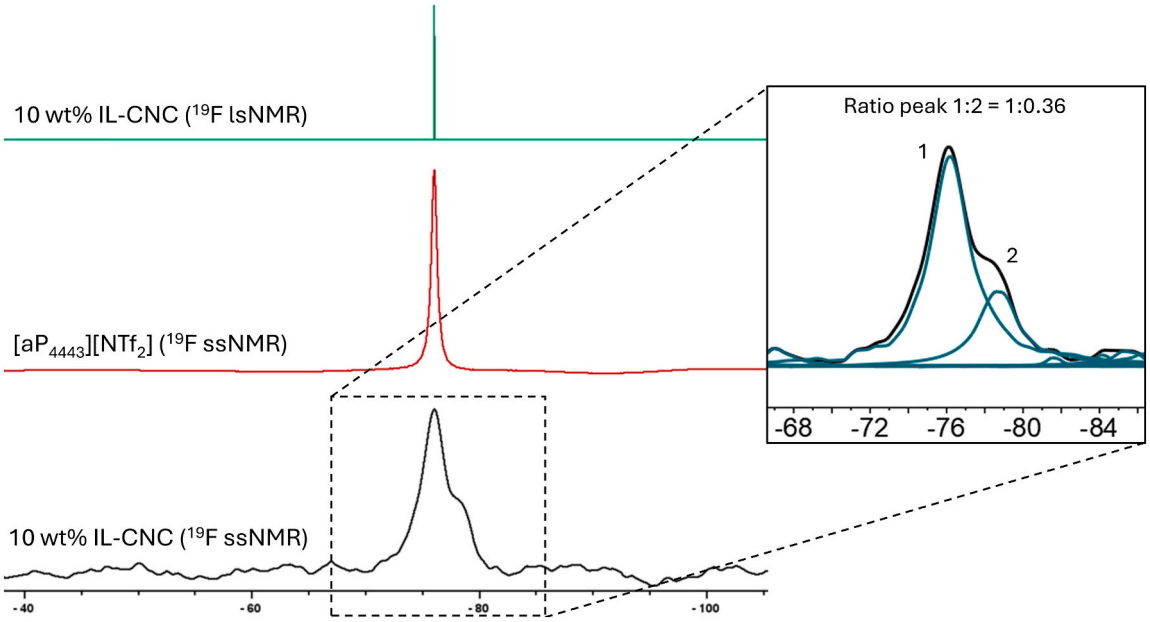

Fig. 5. ^{19}F solid-state NMR spectra of 10 wt% IL-CNC and $[aP_{4443}[NTf_2]$, and ^{19}F solution-state NMR spectrum of 10 wt% IL-CNC in DMSO-d_6. (Inset is the deconvolution peak of the 10 wt% IL-CNC (^{19}F ssNMR) showing contributions of ionically interacting and absorbed fluorine in a ratio 1:0.36).

reductive amination reaction. ^{1}H-^{31}P CP/MAS spectra of 10 wt% IL-CNC and 10 wt% IL-CNF (Fig. S3) showed the presence of a single peak at ca. 36.7 ppm in both samples which is attributed to the presence of the phosphorous in the cation of $[aP_{4443}][NTf_2]$ contained in the modified CNMs.

To further investigate the efficiency of the reductive amination of $[aP_{4443}][NTf_2]$ and the CNCs, The degree of surface functionalization (DSF) of the modified CNCs was calculated using Eq. S1 and the results obtained are presented in Fig. S4 (a to g) in the form of spectra deconvolution images (Nigmatullin et al., 2020; Onyianta et al., 2022; G. Xu et al., 2022). The results showed that the DSF values of 1 wt% IL-CNC, 3 wt% IL-CNC, 10 wt% IL-CNC, 20 wt% IL-CNC, 50 wt% IL-CNC and Blank 10 wt% IL-CNC were 0.94 %, 1.71 %, 2.49 %, 2.98 %, 2.52 % and 1.34 % respectively. (Fig. 4 a to g). The values obtained suggest that the modified CNCs from reductive amination of $[aP_{4443}][NTf_2]$ increased by increasing the molar ratio of $[aP_{4443}][NTf_2]$ reacted from 1 wt% to 20 wt % but decreased slightly on a further increase to 50 wt%. The decrease in DSF is probably due to the increase in viscosity observed during the modification reaction of the 50 wt% IL-CNC, limiting the mass transfer process. Furthermore, the DSF value obtained for the Blank 10 wt% IL-

CNC (1.38 %) was lower than the DSF obtained from 10 wt% IL-CNC by reductive amination reaction (2.49 %) (Fig. S4 c & f). This shows that reductive amination between the oxidized CNCs and amine is necessary to optimise the modification reaction.

With regards to the modified CNFs (IL-CNF), as shown in Fig. 4 b, typical cellulose spectra similar to the modified CNCs were observed with the trace presence of only the carbon chains (CH_3/CH_2) from the cation moiety in [aP_{4443}][NTf_2]. In addition, the C6 peaks from the CNFs appeared broad and could be due to a slightly disordered surface. The DSF of 10 wt% IL-CNF calculated from Fig. S4 e was found to be rather low at 0.28 % which is an indication of a poor absorption of [aP_{4443}][NTf_2] on the CNF surface, probably as a result of agglomeration and low surface area of the fibres compared to the 10 wt% IL-CNCs. The lower DSF of the 10 wt% IL-CNF explains the low influence of [aP_{4443}][NTf_2] on the thermal degradation, dispersibility and water contact angle obtained for the modified CNFs later discussed in Sections 3.4 and 3.5.

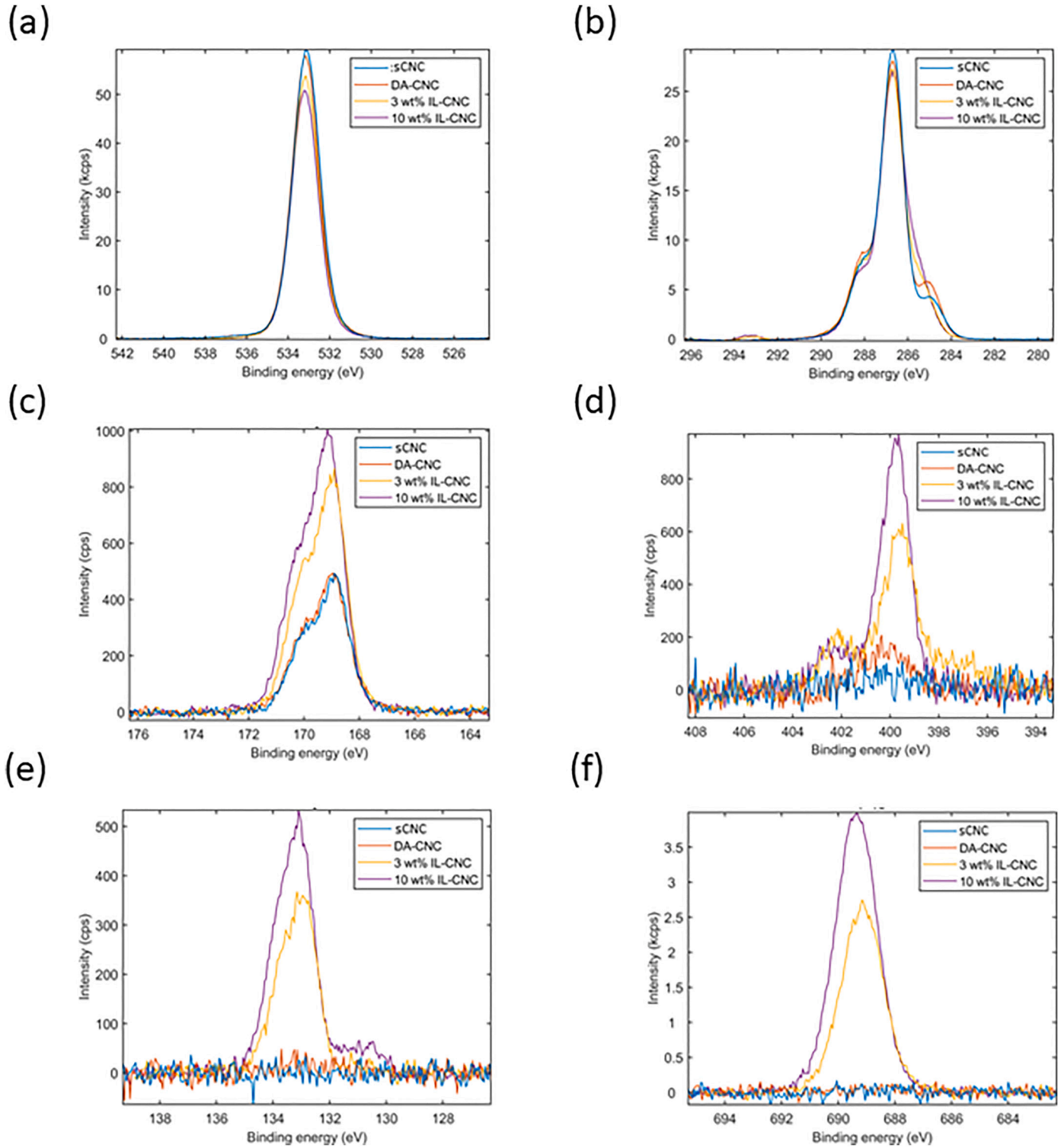

Fig. 6. XPS spectra showing regions of elements found in CNC samples; (a) Oxygen 1s (b) Carbon 1s (c) Sulfur 2p (d) Nitrogen 1s (e) Phosphorous 2p (f) Fluorine 1s.

3.2.3. X-ray photoelectron spectroscopy (XPS)

CNMs were analysed using XPS and the regions observed are presented in Figs. 6 and 7, while quantitative analysis is presented in Table S1. For quantification, spectra have been charge referenced to the C—O peak of cellulose (284.7 eV) (Johansson et al., 2020) and background-subtracted using Shirley-type (C 1s, O 1s), linear (P 2p, Cl 2p, F 1s, N 1s) or quadratic (S 2p) backgrounds. C 1s regions were fitted with 4 or 5 (where CF_3 bonds were present) component models, consisting of Voigt functions constrained to have identical line shapes (Fig. S5 and Table S2 for CNCs and Fig. S6 and Table S3 for CNFs).

From the CNC spectral analysis presented in Fig. 6, it was observed that the O 1s peak centred at 533.2 eV was similar across all the CNC samples and is consistent with both C—O and C═O environments in cellulose (Johansson et al., 2020) (Fig. 6a). Similar amounts of carbon

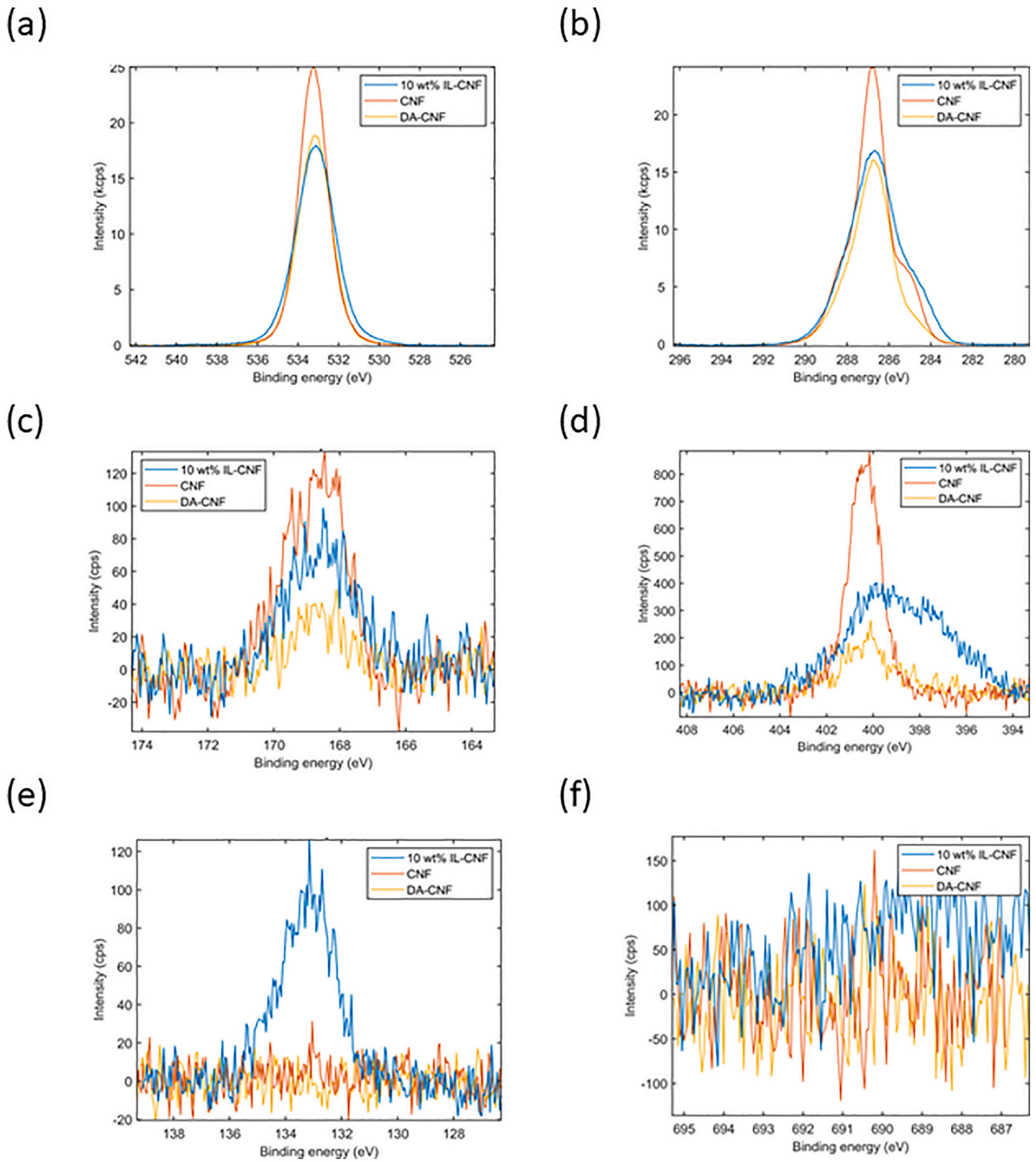

Fig. 7. XPS spectra showing regions of elements found in CNF samples; (a) Oxygen 1s (b) Carbon 1s (c) Sulfur 2p (d) Nitrogen 1s (e) Phosphorous 2p (f) Fluorine 1s.

were obtained for all the CNCs. The C 1s region is typical of a cellulose spectrum (Fig. 6b), indicating several peaks in the samples with the main peak at 286.7 eV attributed to the presence of C—O, a shoulder at 288.3 eV is due to the O-C-O environment, and a weaker shoulder at 289.3 eV which was found to be more prominent in DACNC due to presence of C═O from oxidation. A third shoulder around 285.3 eV due to non-cellulosic C—C and C—N bonds probably at the surface is found to be prominent for 3 wt% IL-CNC and 10 wt% IL-CNC but weak and at a slightly different binding energy in sCNC and DACNC. The change in this peak for 3 wt% IL-CNC and 10 wt% IL-CNC is consistent with the additional C—C and C—N environments of the $[aP_{4443}][NTf_2]$. Furthermore, 3 wt% IL-CNC and 10 wt% IL-CNC displayed an additional peak near 293 eV, attributed to the CF_3 environment in $[aP_{4443}][NTf_2]$ confirming the surface modification of the CNCs.

S 2p with binding energies consistent with the sulfate environment was found in all the CNC samples (Fig. 6c). Binding energies (S $2p_{3/2}$) of 168.9 eV from sulfate half-ester groups appeared for sCNC and DACNC samples, but were found to shift slightly to 169.1 eV and increase in relative intensity for both 3 wt% and 10 wt% IL-CNCs. The higher sulfur content in 3 wt% IL-CNC and 10 wt% IL-CNC reflects the additional presence of sulfonate groups contributed by the $[NTf_2]^-$ anion in the $[aP_{4443}][NTf_2]$.

N 1s which is consistent with amine and oxygen-rich N environments (Le Gars et al., 2020) appeared at 399.7 eV and 402.2 eV in both 3 wt% and 10 wt% IL-CNCs (Fig. 6d). We associate these peaks with the amine group (399.7 eV) and amide (402.2 eV) covalent linkage between the CNCs and $[aP_{4443}][NTf_2]$. A very small and indistinct peak at 400.3 eV was also found for DACNCs, which could be due to atmospheric contamination (e.g., adsorbed N_2).

P 2p signal with binding energy (P $2p_{3/2}$) of 132.9 eV which is consistent with a phosphonium environment (Blundell & Licence, 2014) from the$[aP_{4443}][NTf_2]$ appeared only in 3 wt% and 10 wt% IL-CNCs; namely at 0.6 and 0.9 % respectively (Fig. 6e). F 1s was observed at binding energies of 689.2 eV and 689.4 eV for both 3 wt% and 10 wt% IL-CNC, respectively (Fig. 6f). The percentage composition of F was found to be 1.7 % and 2.5 % in 3 wt% and 10 wt% IL-CNC respectively (Table S1). This is consistent with the presence the fluorinated $[aP_{4443}][NTf_2]$ in these samples.

With regards to the CNFs, both modified and unmodified CNFs contained oxygen, carbon, sulfur and nitrogen signals (Figs. 7a to d respectively, and Table S1). The N 1s spectrum of 10 wt% IL-CNF (Fig. 7d) was found to be much broader than that of the CNCs, indicating either a range of mixed chemical environments or, more likely, differential charging of the fibres. In topographically complex structures of non-conducting materials, the surface can acquire spatially varying local charge during the photoemission process, leading to small electric fields near the surface that broaden the energy resolution of the XPS measurement for this example. The evidence of surface modification of the CNF can be seen in the C 1s signal which contains a much greater contribution at 284.8 eV for 10 wt% IL-CNF, indicating additional non-cellulosic C—C and C—N environments in $[aP_{4443}][NTf_2]$ at the CNF surface (Fig. 7b). Furthermore the P 2p signal (Fig. 7e), which was absent in unmodified CNF and DACNF, was only present in the 10 wt% IL-CNF and is an indication of $[aP_{4443}][NTf_2]$ from the modification process.

A contribution from F 1s due to $[aP_{4443}][NTf_2]$ is expected to be present in the modified CNF but was not detected (Fig. 7f). The reason for this could be due to the fact that the $[NTf_2]^-$ anion is highly delocalised and interacts poorly with the phosphonium cation thereby possessing enhanced ion mobility in a way that this anion becomes capable of changing conformations from the surface to within the core of the CNF which cannot be detected by XPS. XPS is sensitive to roughly the uppermost 10 nm of the material surface, which is smaller than a typical fibril diameter. In addition, the rather low concentration of $[aP_{4443}][NTf_2]$ on the surface of the CNFs, as verified by the DSF of 0.28 % obtained from NMR analysis (Section 3.2.2), could explain the inability for fluorine to be detected in the modified materials.

3.2.4. X-ray diffraction analysis

The effect of surface modification on the crystalline structures of the CNMs was determined by XRD analysis. The diffraction patterns are displayed in Fig. 8 while their corresponding crystallinity indices, calculated using Eq. 1, are presented in Table S4.

The crystalline structure of sCNC in Fig. 8a showed 5 distinct Bragg peaks at 2θ =12.2°, 15.1°, 20.1°, 22.6°, 34.4 assigned to $1^{-}10$, 110, 021/120, 200 and 004 planes of the cellulose I crystalline structure respectively (Lin & Dufresne, 2014), and an additional small peak located at 38.4°. The crystallinity index of sCNC was found to be 94.2 %. After modification of sCNC, a similar diffraction pattern was observed. However, 3 wt% IL-CNC and 10 wt% IL-CNC both exhibited a decrease in intensity and a slight variation in the position of Bragg peaks, with the absence of the peak at 38.48° for 10 wt% IL-CNC. Furthermore, crystallinity indices of 87.7 % for 3 wt% IL-CNC and 90.6 % for 10 wt% IL-CNC were obtained. The results are an indication of a slight alteration to the crystalline structure of the CNCs due to surface modification.

The XRD pattern of the unmodified and modified CNFs were similar with Bragg peaks located at 2θ =16.1°, 22.6° and 34.9° assigned to the $1^{-}10$, 200 and 004 planes of a cellulose I crystal structure respectively (Almasi et al., 2015) (Fig. 8b). The intensities of these peaks were found to decrease after surface modification while the crystallinity index of CNF which was 85.7 % increased to 90.7 % for 10 wt% IL-CNF. The high degree of crystallinity of the CNF could result in a compact fibre structure with restricted access to hydroxy groups for modification with $[aP_{4443}][NTf_2]$ (Almasi et al., 2015) which could be responsible for the low DSF obtained for the 10 wt% IL-CNF. Overall, these results suggests that the surface modification of CNF with $[aP_{4443}][NTf_2]$ did not have much effect on the inherent structure of the CNFs but resulted to an increase in their crystallinity.

3.3. Effect of modification on morphology of CNMs

TEM images of unmodified and modified CNMs are presented in Fig. 9, with their dimensions reported in Table S5. The length and widths of individual sCNCs, 3 wt% and 10 wt% IL-CNCs are in agreement with other values reported in the literature (Dong et al., 1998; Le Gars et al., 2020; Robert J. Moon et al., 2011). The CNC samples were found to retain their typical rodlike morphology, with no significant change in size after modification. However, after surface modification with $[aP_{4443}][NTf_2]$, aggregation of the CNCs occurred, which was more noticeable at higher mass fractions of the $[aP_{4443}][NTf_2]$. The aggregation observed supports the idea that the presence of even a small amount of fluorine on the surface of the modified CNCs completely changes the surface chemistry and thereby interactions between the materials. This observation is similar to previous reports on surface modification of CNCs with hydrophobic groups (Nigmatullin et al., 2020; Onyianta et al., 2022; Tang et al., 2018; G. Xu et al., 2022).

The TEM images of unmodified and modified CNF (Fig. 9d & e) indicates that widespread aggregation of nanofibers occurred making it difficult to obtain widths of single isolated fibrils. As shown in Table S4, The average widths of the unmodified CNFs was found to be 30.9 ± 39.0 nm with minimum and maximum widths of 5.1 and 116.8 nm respectively, while the average width of the 10 wt% IL-CNF was 28.7 ± 38.9 nm, with minimum and maximum widths of 4.7 and 186.7 nm respectively. The minimum fibril widths are within the range of previous reports on CNFs (Isogai et al., 2011). Our results suggest that the original morphology and arrangements of the fibrils was not affected by surface modification.

3.4. Effect of modification on surface properties

3.4.1. Conductometric titrations

Sulfate half-ester groups introduced on the surface of CNCs during

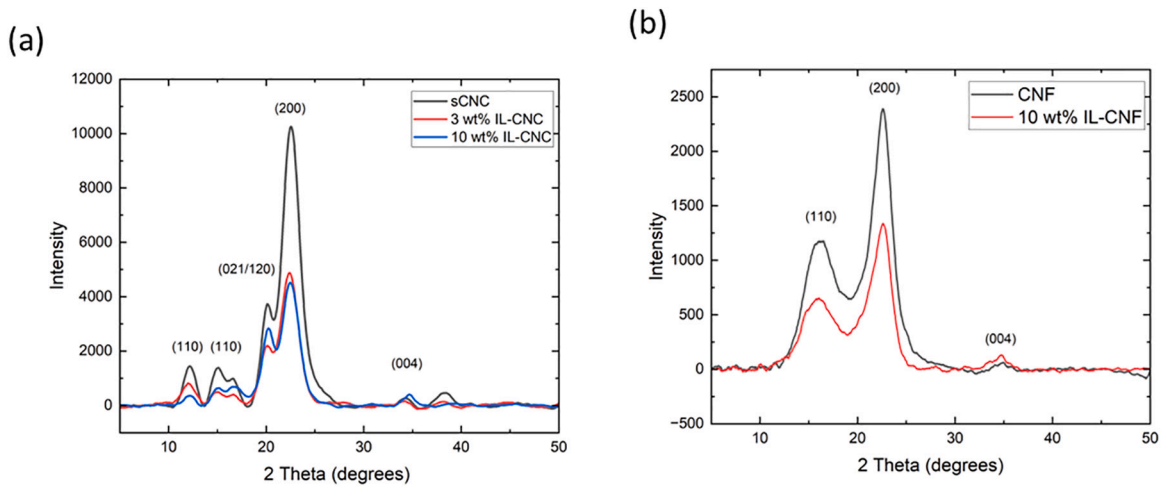

Fig. 8. X-ray diffractograms of unmodified and modified (a) CNCs and (b) CNFs.

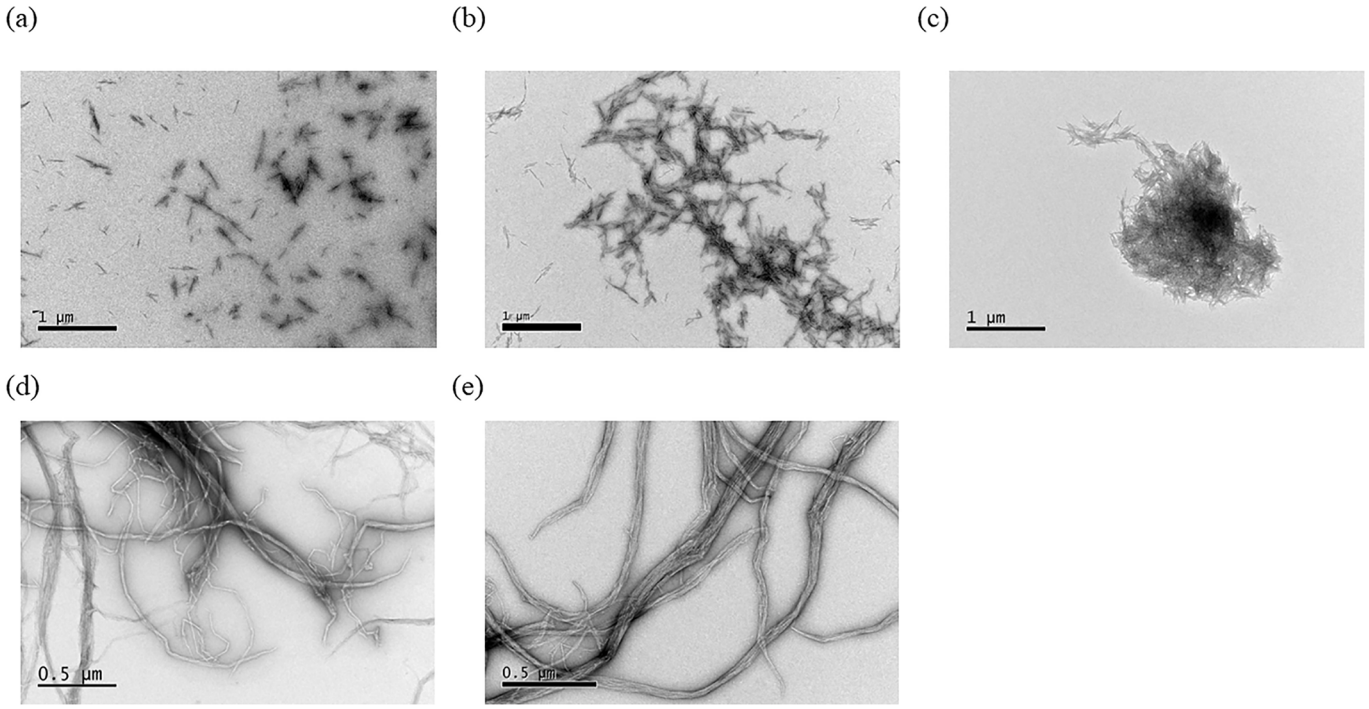

Fig. 9. Representative TEM images of (a) unmodified sCNCs, (b) 3 wt% IL-CNCs, (c) 10 wt% IL-CNCs, (d) unmodified CNFs, (e) 10 wt% IL-CNFs.

the extraction with sulfuric acid hydrolysis is a fundamental feature that contributes to the colloidal stability and electrostatic behaviour of nanocrystals in solution (Beck et al., 2015). Surface modification of CNCs often utilizes the hydroxy, sulfate half-ester groups, or the reducing end groups (Eyley & Thielemans, 2014). Reductive amination is thought to graft the ionic liquids to the dialdehyde groups on the C2 and C3 of the cellulose structure; the surface charge density obtained from the sulfate half-ester groups on the C6 carbon by conductometric titration should therefore remain the same. However, conductivity, which is the basis for conductometric titration, depends on the concentration of many ions present in the solution and thus could be influenced by the presence of the $[aP_{4443}][NTf_2]$ on the surface of CNCs. The surface charges obtained by conductometric titration of the sCNCs, 3 wt% IL-CNCs and 10 wt% IL-CNCs were 448.6 ± 8.3, 113.8 ± 2.3 and 224.1 ± 0.1 mmol kg^{-1} respectively. These data are plotted in Fig. 10 and suggest that surface modification of the sCNCs with the $[aP_{4443}][NTf_2]$ ionic liquid resulted in a substantial reduction in the surface charge values of sCNCs by approximately 75 % for 3 wt% IL-CNC and 50 % for 10 wt% IL-CNC. The implication is that the sulfate half-ester groups are shielded by the presence of $[aP_{4443}][NTf_2]$ on the CNCs. The values obtained for the surface charges in the 3 wt% and 10 wt% IL-CNC samples suggest that the 10 wt% IL-CNC suspension made a greater contribution to the total surface charge than the 3 wt% IL-CNC probably due to the fact that ionic conductivity would naturally increase with an increase in the concentration of ions (De Sarkar et al., 2020). With respect to the CNF derivatives, this investigation was not performed since there are no sulfate half ester groups present for this form of CNM.

3.4.2. *Zeta potential and stability of colloidal suspensions*

To further understand the effect of surface modification on the colloidal stability of the CNM suspensions in water, photographs at various settling times (0–24 h) were taken of freshly dispersed and

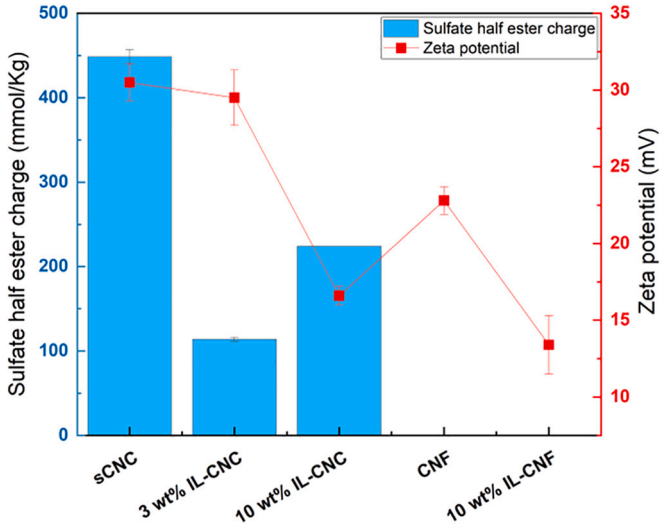

Fig. 10. Surface half ester charges and zeta potential of modified CNMs.

sonicated samples; these are presented in Fig. 11. The images clearly show that the sCNCs and 3 wt% IL-CNC (Fig. 11, vials a & b) formed a stable colloidal suspensions over time while 10 wt% IL-CNC (vial c) began settling to the bottom of the vial 15 min after dispersion and gradually over a 24 h period.

With respect to the CNF suspensions (Fig. 11; vials d & e), unmodified CNF (vial d) remained stable up to 30 min after dispersion, while the 10 wt% IL-CNF (Fig. 11, vial e) began to form aggregates and settled rapidly 15 min after dispersion and completely by forming a clear aqueous upper phase after a settling time of 30 mins. The dispersion effect is likely due to strong repulsions between water molecules and $[aP_{4443}][NTf_2]$ on the surface of the 10 wt% IL-CNCs and 10 wt% IL-CNF respectively, as seen with other charged CNMs (Salam et al., 2015). The decreased water affinity observed in the modified CNMs compared to their unmodified counterparts is due to the ability of fluorine in $[aP_{4443}][NTf_2]$ to cause significant changes in surface energy reducing adhesion to hydrophilic substances (Salam et al., 2015). This effect was not observed for the 3 wt% IL-CNC as the concentration of $[aP_{4443}][NTf_2]$ is thought to be too low.

Zeta potential is an indicator of the stability of colloidal suspensions, and was determined to assess the dispersibility of the unmodified and modified CNMs in an aqueous medium. Generally Zeta potential values of >30 mV are indicative of a suspension with good colloidal stability, from 10 to 30 mV those with insipient stability, while values <10 mV corresponds to a low stability. These latter suspensions will tend to flocculate over time (Everett & Sankey, 1988). Zeta potential values obtained are plotted in Fig. 10, along-side their sulfate half ester charge. Zeta potential values of CNCs, which were found to be colloidally stable, reported a value of -30.5 ± 1.2 mV. The stability of CNCs, with similar surface charge, has been attributed to the negatively charged sulfate half-ester groups (Llàcer Navarro et al., 2021). After surface modification with $[aP_{4443}][NTf_2]$, Zeta potential values remained the same at -29.5 ± 1.8 mV for the 3 wt% IL-CNC, but substantially increased to a value of -16.6 ± 0.6 mV for the 10 wt% IL-CNC. These results suggest that the grafting of 3 wt% $[aP_{4443}][NTf_2]$ to the sCNC had a negligible effect on the charge emanating from the sulfate half ester groups, retaining their colloidal stability, and in support of what was observed in Fig. 11. The increase in surface modification to 10 wt% resulted in a loss of stability, probably due to a charge screening effect by the ionic liquid anion. It should be noted that the $[NTf_2]^-$ anion is poorly co-ordinated with its large size (De Sarkar et al., 2020), and is capable of causing this kind of screening effect. This charge screening effect is common for modified sCNC with large groups and is in agreement with similar reports on the effect of surface modification with large groups such as

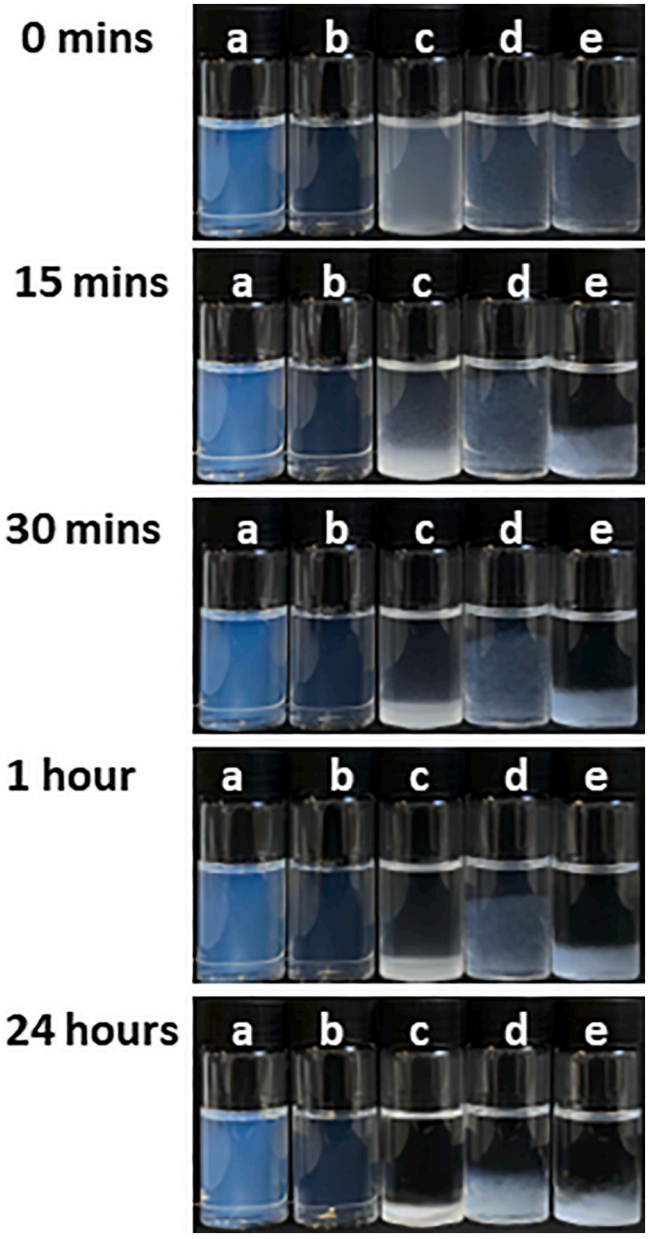

Fig. 11. Digital images of (a) sCNC, (b) 3 wt% IL-CNC, (c) 10 wt% IL-CNC, (d) CNF, (e) 10 wt% IL-CNF showing the colloidal stability of the dispersions at various settling times. Concentrations were kept at 0.05 wt%.

octylamine (Onyianta et al., 2022). However, we aim to address this here by retaining charge, and water dispersibility while also providing hydrophobic groups that could interact with other materials with similar surface activity. The Zeta potential for CNF before and after surface modification with 10 wt% IL was found to be -22.8 ± 0.9 mV and -13.4 ± 1.9 mV respectively and similar conclusions with respect to the charge screening effect observed for the CNCs by the $[aP_{4443}][NTf_2]$ can be inferred. The changes in colloidal stability observed for the modified CNMs are an indication that the $[aP_{4443}][NTf_2]$ was successfully grafted onto the surface of the CNMs in various amounts via the cation by reductive amination.

3.4.3. *Water contact angle (WCA)*

The WCAs of the CNMs were measured to examine the effect of the attached $[aP_{4443}][NTf_2]$ on the hydrophobicity of the samples. The results obtained are reported as averages from dynamic water contact

angles presented in Fig. 12. Prior to modification with the [aP_{4443}][NTf_2], the sCNC films which contain sulfate half ester groups were found to be hydrophilic with WCAs of 27.5 ± 1.5°. After modification with various amounts of [aP_{4443}][NTf_2], WCAs of 40.4 ± 2.4° and 54.0 ± 7.6° for 3 wt% and 10 wt% IL-CNCs were obtained respectively. Similar results have been reported for sulfated CNCs and modified forms with hydrophobic groups (Ly & Mekonnen, 2020; Onyianta et al., 2022; Wei et al., 2018).

With respect to the surface modification of CNFs, the unmodified CNF and 10 wt% IL-CNF exhibited WCAs of 41.5 ± 6° and 51.9 ± 3.2° respectively. The results obtained for the unmodified CNF is in agreement with previous reports (Ishida & Kondo, 2023). Fluorinated functional groups on the surface of CNMs are expected to enhance their hydrophobicity (Khanjani et al., 2018; Salam et al., 2015). This was evident in the changes in WCAs of the CNMs after surface modification with [aP_{4443}][NTf_2], thereby confirming the presence of [aP_{4443}][NTf_2] on the CNMs. However, as shown in Fig. 12, the results obtained are mid-range hydrophobicity and indicates that the CNMs still possessed some hydrophilic properties at their current DSF (Section 3.2.2) probably as a result of the slight modification or incomplete derivatization of neighbouring (exposed) hydroxy groups. Interestingly, what is noticeable is the pronounced difference in the surface wettability between the CNCs and CNFs before and after modification, which is probably related to the nature of the individual CNMs. The CNCs have a more ordered surface region while the CNFs have lower ordered surface regions.

Overall, the results suggest the possibility of obtaining higher WCA of the CNMs by increasing the degree of functionalization of [aP_{4443}][NTf_2] on the CNM surface.

3.5. *Effect of modification on thermal degradation properties of CNC and CNF*

Thermal stability is an important factor considered in determining potential applications of CNMs, particularly for composite materials where these materials may be combined with polymer matrices with high melting points. Therefore, the thermal stability of the unmodified and modified CNMs were measured and compared to ascertain the effect of surface modification on this important property. Data were plotted as mass loss against temperature and derivative thermogravimetric (DTG) against temperature as shown in Fig. 13, while the physical parameters from these data are presented in Table S7.

Generally, ionic liquids possess remarkable thermal stabilities and in particular ionic liquids with a [NTf_2]$^-$anion (Pringle et al., 2003). As shown in Table S7 and thermograms in Fig. 13, the [aP_{4443}][NTf_2] ionic liquid employed for the surface modification in this study was found to have its onset degradation at ~380 °C and peak degradation at 436 °C.

For the CNC derivatives (Fig. 13 a and c) the respective onset degradation temperatures of sCNC, 3 wt% IL-CNCs, and 10 wt% IL-CNCs are ~232, ~250, and ~275 °C respectively. Observation of the DTG curves of the CNCs showed two peak degradation temperatures for sCNCs at ~252 °C and ~297 °C, both of which are associated with the degradation of the sulfated and non-sulfated regions of the materials respectively (D'Acierno et al., 2020; Merlini et al., 2020; Onyianta et al., 2022; Roman & Winter, 2004). For the 3 wt% and 10 wt% IL-CNCs only single peak degradation curves at ~286 and 310 °C were observed respectively. Our results demonstrate significant increases in the thermal stability of the CNCs, with a systematic increase in the degree of surface functionalization of [aP_{4443}][NTf_2] on the modified CNCs. This observation is probably due to the ability of the [aP_{4443}][NTf_2] to provide insulation on the surface of the modified CNCs when heated. This could have significant benefits for these materials to be applied in high temperature composite materials, and as polymer gel electrolytes in batteries.

With regards to the CNF derivatives, (Fig. 13 b and d) the onset of thermal degradation for CNF and 10 wt% IL-CNF was found to be the same at ~270 °C and the peak degradation temperatures of CNF and 10 wt% IL-CNF were at ~350 °C and ~339 °C respectively. Although CNFs are generally more stable than CNCs due to the absence of heat-sensitive surface groups such as sulfate half-esters (D'Acierno et al., 2023), the impact of grafting the [aP_{4443}][NTf_2] on the CNF slightly decreased the degradation temperature. Similar decreases in thermal stability have been reported for surface modified CNFs, which have been attributed to a reduction in the crystallinity of the fibrils after modification (Almasi et al., 2015; Balasubramaniam et al., 2020; Jandura et al., 2000). It is thought that substituting the surface hydroxy groups with hydrophobic groups decreases the crystallinity of cellulose, resulting in a reduced thermal stability (Balasubramaniam et al., 2020), however, the crystallinity of the CNFs was found to increase after modification thus this remains a topic for future research. In addition, the low DSF obtained for the 10 wt% IL-CNF implies a negligible influence of [aP_{4443}][NTf_2] on its thermal degradation properties.

Overall, the results obtained for CNF prior to modification are in agreement with previous reports (D'Acierno et al., 2020).

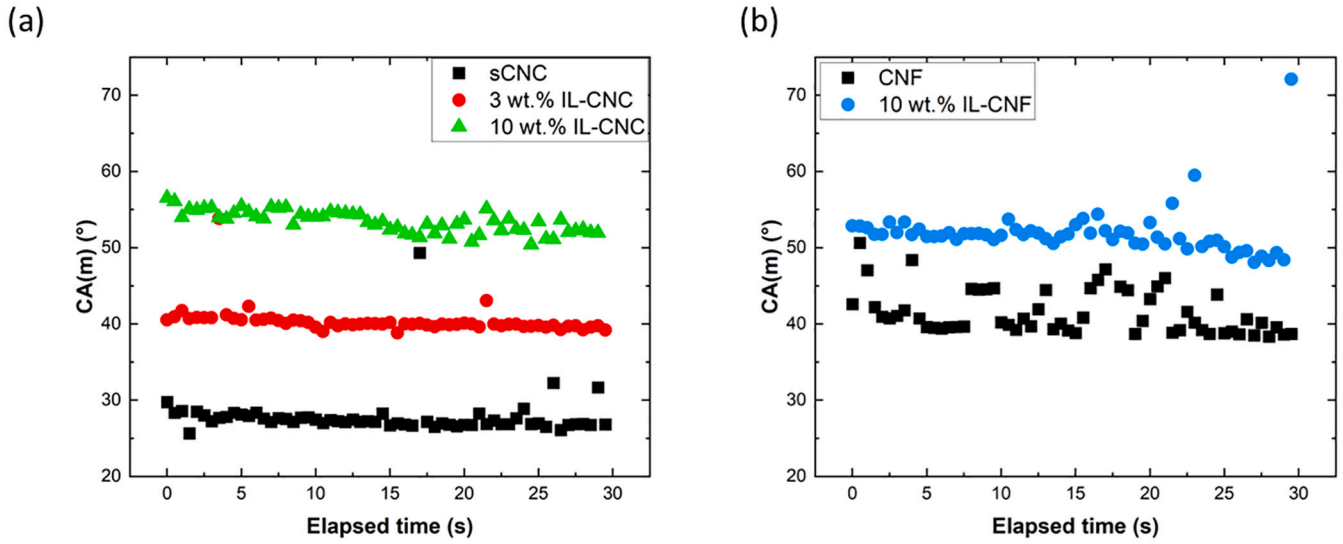

Fig. 12. Dynamic water contact angles of modified and unmodified (a) CNC and (b) CNFs.

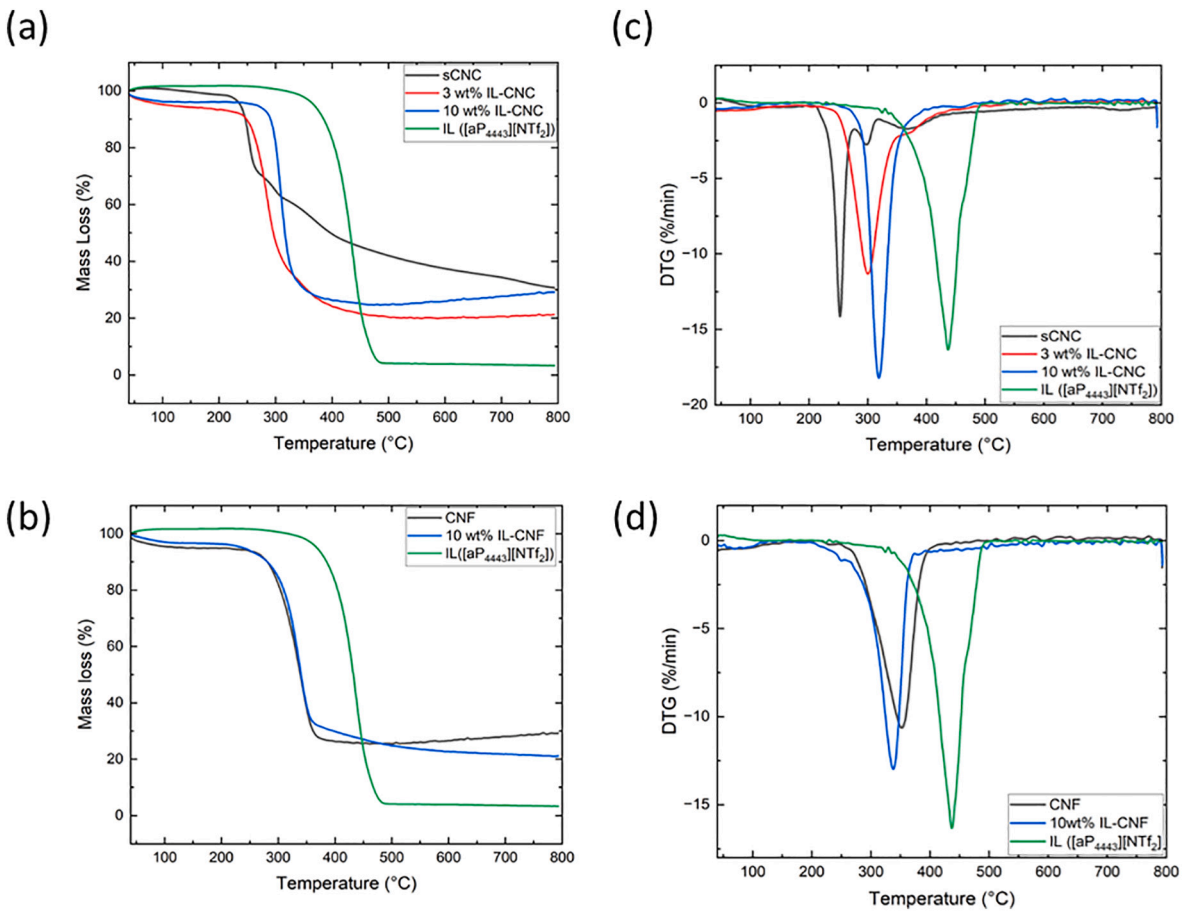

Fig. 13. Thermal Gravimetric Analysis (TGA) thermograms of (a) CNCs, (b) CNFs and Differential Thermal Gravimetric (DTG) thermograms of (c) CNCs, (d) CNFs.

4. Conclusions

A highly hydrophobic ionic liquid known as 3-aminopropyltributyl-phosphonium bis(trifluoromethylsulfonyl)imide ([aP_{4443}][NTf_2]) was synthesized and applied for the first time for the hydrophobization of CNMs. The chemical surface modification route was performed in two steps involving oxidation of the CNMs and a subsequent reductive amination with various concentrations of [aP_{4443}][NTf_2] grafted on the CNM surfaces by amide bonds. Characterization of the [aP_{4443}][NTf_2] modified CNMs by XPS, NMR, XRD, Zeta potential, conductometric titration, TEM, TGA, and contact angle analysis gave sufficient evidence of the presence of the [aP_{4443}][NTf_2] on the surface of the modified CNMs when compared with their unmodified counterparts leading to moderately hydrophobized CNMs. This is important to achieve, since often over-modification of cellulose, particularly charged forms, can reduce their ability to be dispersed in water. Our unique approach to this enables some amphiphilicity to the CNMs.

Thermal degradation was significantly increased for modified CNCs, demonstrating their potential for use in composites materials at high temperatures. CNFs however exhibited a slight reduction in the thermal stability, which is thought to be due to low DSF of [aP_{4443}][NTf_2]. The properties obtained for these functionalised celluloses was attributed to the hydrophobicity and thermal stability of the [aP_{4443}][NTf_2] enabled by tributyl chains and fluorinated anions. This work makes a significant contribution to the research efforts in applying green chemicals in the form of ionic liquids and opens more opportunities for safely enhancing the properties of CNMs to achieve hydrophobic CNMs suitable for aqueous processing with thermoplastics, the fabrication of thermally stable composite materials, and for their use as polymer gel electrolytes in batteries.

CRediT authorship contribution statement

Onajite T. Abafe Diejomaoh: Writing – review & editing, Writing – original draft, Visualization, Validation, Methodology, Investigation, Formal analysis, Data curation, Conceptualization. **Alessandra Lavoratti:** Writing – review & editing, Visualization, Validation, Investigation, Formal analysis. **Jude Laverock:** Writing – review & editing, Supervision, Investigation, Formal analysis, Data curation. **Todor T. Koev:** Writing – review & editing, Supervision, Software, Methodology, Investigation, Formal analysis, Data curation. **Yaroslav Z. Khimyak:** Writing – review & editing, Validation, Supervision, Funding acquisition, Formal analysis. **Tetsuo Kondo:** Writing – review & editing, Visualization, Supervision, Resources, Formal analysis. **Stephen J. Eichhorn:** Writing – review & editing, Methodology, Investigation, Funding acquisition, Formal analysis, Conceptualization.

Declaration of competing interest

None.

Data availability

Data generated from this work is freely available from the University of Bristol's repository at https://data.bris.ac.uk/data/.

Acknowledgements

This work was financially supported by an Engineering and Physical Sciences Research Council ED&I Fellowship (EP/V002651/1) and an Overseas Travel Grant (EP/T005831/1). TK is funded via a UKRI Future

Leaders Fellowship awarded to Dr. Matthew Wallace (MR/T044020/1). TK and YK are grateful to the UEA Faculty of Science NMR facility.

Appendix A. Supplementary data

Supplementary data to this article can be found online at https://doi.org/10.1016/j.carbpol.2024.122519.

References

Abafe Diejomaoh, O. T., Inyang, V. M., & Azim, M. M. (2023). A complete study on the synthesis of ionic liquids. In J. Akhter Siddique, A. Ahmad, & M. Jawaid (Eds.), *Ionic liquids and their application in green chemistry* (pp. 13–26). Elsevier.

Abitbol, T., Kloser, E., & Gray, D. G. (2013). Estimation of the surface sulfur content of cellulose nanocrystals prepared by sulfuric acid hydrolysis. *Cellulose, 20*, 785–794.

Alila, S., Ferraria, A. M., & Botelho do Rego, A. M., & Boufi, S.. (2009). Controlled surface modification of cellulose fibers by amino derivatives using N,N′-carbonyldiimidazole as activator. *Carbohydrate Polymers, 77*(3), 553–562.

Almasi, H., Ghanbarzadeh, B., Dehghannia, J., Pirsa, S., & Zandi, M. (2015). Heterogeneous modification of softwoods cellulose nanofibers with oleic acid: Effect of reaction time and oleic acid concentration. *Fibers and Polymers, 16*, 1715–1722.

Balasubramaniam, S. L., Patel, A. S., & Nayak, B. (2020). Surface modification of cellulose nanofiber film with fatty acids for developing renewable hydrophobic food packaging. *Food Packaging and Shelf Life, 26*, Article 100587.

Beaumont, M., Bacher, M., Opietnik, M., Gindl-Altmutter, W., Potthast, A., & Rosenau, T. (2018). A general aqueous silanization protocol to introduce vinyl, mercapto or azido functionalities onto cellulose fibers and nanocelluloses. *Molecules, 23*(6), 1427.

Beck, S., Méthot, M., & Bouchard, J. (2015). General procedure for determining cellulose nanocrystal sulfate half-ester content by conductometric titration. *Cellulose, 22*(1), 101–116.

Bideau, B., Loranger, E., & Daneault, C. (2018). Nanocellulose-polypyrrole-coated paperboard for food packaging application. *Progress in Organic Coatings, 123*, 128–133.

Blundell, R. K., & Licence, P. (2014). Quaternary ammonium and phosphonium based ionic liquids: A comparison of common anions. *Physical Chemistry Chemical Physics, 16*(29), 15278–15288.

Bradaric, C. J., Downard, A., Kennedy, C., Robertson, A. J., & Zhou, Y. (2003). Industrial preparation of phosphonium ionic liquids. *Green Chemistry, 5*(2), 143–152.

Camplo, M., Wathier, M., Chow, J., & Grinstaff, M. W. (2011). A versatile reagent to synthesize diverse ionic liquids ranging from small molecules and dendrimers to functionalized proteins. *Chemical Communications, 47*(7), 2128–2130.

Casarano, R., & El Seoud, O. A. (2013). Successful application of an ionic liquid carrying the fluoride counter-ion in biomacromolecular chemistry: Microwave-assisted acylation of cellulose in the presence of 1-allyl-3-methylimidazolium fluoride/DMSO mixtures. *Macromolecular Bioscience, 13*(2), 191–202.

Cellante, L., Costa, R., Monaco, I., Cenacchi, G., & Locatelli, E. (2018). One-step esterification of nanocellulose in a Brønsted acid ionic liquid for delivery to glioblastoma cancer cells. *New Journal of Chemistry, 42*(7), 5237–5242.

D'Acierno, F., Hamad, W. Y., Michal, C. A., & MacLachlan, M. J. (2020). Thermal degradation of cellulose filaments and nanocrystals. *Biomacromolecules, 21*(8), 3374–3386.

D'Acierno, F., Michal, C. A., & MacLachlan, M. J. (2023). Thermal stability of cellulose nanomaterials. *Chemical Reviews, 123*(11), 7295–7325.

Dash, R., Elder, T., & Ragauskas, A. J. (2012). Grafting of model primary amine compounds to cellulose nanowhiskers through periodate oxidation. *Cellulose, 19*(6), 2069–2079.

De Sarkar, S., Mitra, S., & Ghosh, S. K. (2020). Relating the physical properties of aqueous solutions of ionic liquids with their chemical structures. *The European Physical Journal E, 43*(8), 55.

Dong, X. M., Revol, J.-F., & Gray, D. G. (1998). Effect of microcrystallite preparation conditions on the formation of colloid crystals of cellulose. *Cellulose, 5*(1), 19–32.

Earle, M. J., Esperança, J. M., Gilea, M. A., Canongia Lopes, J. N., Rebelo, L. P., Magee, J. W., … Widegren, J. A. (2006). The distillation and volatility of ionic liquids. *Nature, 439*(7078), 831–834.

Eichhorn, S. J., Etale, A., Wang, J., Berglund, L. A., Li, Y., Cai, Y., … Frka-Petesic, B. (2022). Current international research into cellulose as a functional nanomaterial for advanced applications. *Journal of Materials Science, 57*(10), 5697–5767.

Etale, A., Onyianta, A. J., Turner, S. R., & Eichhorn, S. J. (2023). Cellulose: A review of water interactions, applications in composites, and water treatment. *Chemical Reviews, 123*(5), 2016–2048.

Everett, D. H., & Sankey. (1988). *Basic principles of colloid science*. The Royal Society of Chemistry.

Eyley, S., & Thielemans, W. (2014). Surface modification of cellulose nanocrystals. *Nanoscale, 6*(14), 7764–7779.

Froidevaux, V., Negrell, C., Caillol, S., Pascault, J.-P., & Boutevin, B. (2016). Biobased amines: From synthesis to polymers; present and future. *Chemical Reviews, 116*(22), 14181–14224.

Fukumoto, K., & Ohno, H. (2006). Design and synthesis of hydrophobic and chiral anions from amino acids as precursor for functional ionic liquids. *Chemical Communications, 29*, 3081–3083.

Gericke, M., Schaller, J., Liebert, T., Fardim, P., Meister, F., & Heinze, T. (2012). Studies on the tosylation of cellulose in mixtures of ionic liquids and a co-solvent. *Carbohydrate Polymers, 89*(2), 526–536.

Habibi, Y. (2014). Key advances in the chemical modification of nanocelluloses. *Chemical Society Reviews, 43*(5), 1519–1542.

Ishida, K., & Kondo, T. (2023). Evaluation of surface free energy inducing interfacial adhesion of amphiphilic cellulose nanofibrils. *Biomacromolecules, 24*(8), 3786–3793.

Isogai, A., Saito, T., & Fukuzumi, H. (2011). TEMPO-oxidized cellulose nanofibers. *Nanoscale, 3*(1), 71–85.

Jamil, R., & Silvester, D. S. (2022). Ionic liquid gel polymer electrolytes for flexible supercapacitors: Challenges and prospects. *Current Opinion in Electrochemistry, 35*, Article 101046.

Jandura, P., Riedl, B., & Kokta, B. V. (2000). Thermal degradation behavior of cellulose fibers partially esterified with some long chain organic acids. *Polymer Degradation and Stability, 70*(3), 387–394.

Johansson, L.-S., Campbell, J. M., & Rojas, O. J. (2020). Cellulose as the in situ reference for organic XPS. Why? Because it works. *Surface and Interface Analysis, 52*(12), 1134–1138.

Khanjani, P., King, A. W. T., Partl, G. J., Johansson, L.-S., Kostiainen, M. A., & Ras, R. H. A. (2018). Superhydrophobic paper from nanostructured fluorinated cellulose esters. *ACS Applied Materials & Interfaces, 10*(13), 11280–11288.

Khazalpour, S., Yarie, M., Kianpour, E., Amani, A., Asadabadi, S., Seyf, J. Y., … Zolfigol, M. A. (2020). Applications of phosphonium-based ionic liquids in chemical processes. *Journal of the Iranian Chemical Society, 17*(8), 1775–1917.

Klemm, D., Heublein, B., Fink, H.-P., & Bohn, A. (2005). Cellulose: Fascinating biopolymer and sustainable raw material. *Angewandte Chemie International Edition, 44*(22), 3358–3393.

Kondo, T., Kose, R., Naito, H., & Kasai, W. (2014). Aqueous counter collision using paired water jets as a novel means of preparing bio-nanofibers. *Carbohydrate Polymers, 112*, 284–290.

Le Gars, M., Delvart, A., Roger, P., Belgacem, M. N., & Bras, J. (2020). Amidation of TEMPO-oxidized cellulose nanocrystals using aromatic aminated molecules. *Colloid and Polymer Science, 298*(6), 603–617.

Lin, N., & Dufresne, A. (2014). Surface chemistry, morphological analysis and properties of cellulose nanocrystals with gradiented sulfation degrees. *Nanoscale, 6*(10), 5384–5393.

Liu, S.-H., & Sie, W.-H. (2016). CO2 capture on mesocellular silica foam supported amino acid-functionalized ionic liquids. *Water, Air, & Soil Pollution, 227*(8), 263.

Llàcer Navarro, S., Nakayama, K., Idström, A., Evenäs, L., Ström, A., & Nypelö, T. (2021). The effect of sulfate half-ester groups on cellulose nanocrystal periodate oxidation. *Cellulose, 28*(15), 9633–9644.

Lu, J., Askeland, P., & Drzal, L. T. (2008). Surface modification of microfibrillated cellulose for epoxy composite applications. *Polymer, 49*(5), 1285–1296.

Ly, M., & Mekonnen, T. H. (2020). Cationic surfactant modified cellulose nanocrystals for corrosion protective nanocomposite surface coatings. *Journal of Industrial and Engineering Chemistry, 83*, 409–420.

Lyne, B. (2013). *Market prospects for nanocellulose*. Edmunton, AB, Canada: The Royal Institute of Technology, Alberta Biomaterials Development Centre.

Macarie, L., Simulescu, V., & Ilia, G. (2019). Phosphonium-based ionic liquids used as reagents or catalysts. *ChemistrySelect, 4*(32), 9285–9299.

Majoinen, J., Walther, A., McKee, J. R., Kontturi, E., Aseyev, V., Malho, J. M., … Ikkala, O. (2011). Polyelectrolyte brushes grafted from cellulose nanocrystals using Cu-mediated surface-initiated controlled radical polymerization. *Biomacromolecules, 12*(8), 2997–3006.

Merlini, A., Claumann, C., Zibetti, A. W., Coirolo, A., Rieg, T., & Machado, R. A. F. (2020). Kinetic study of the thermal decomposition of cellulose nanocrystals with different crystal structures and morphologies. *Industrial & Engineering Chemistry Research, 59*(30), 13428–13439.

Moon, R. J., Martini, A., Nairn, J., Simonsen, J., & Youngblood, J. (2011). Cellulose nanomaterials review: Structure, properties and nanocomposites. *Chemical Society Reviews, 40*(7), 3941–3994.

Moon, R. J., Schueneman, G. T., & Simonsen, J. (2016). Overview of cellulose nanomaterials, their capabilities and applications. *Jom, 68*, 2383–2394.

Nechyporchuk, O., Belgacem, M. N., & Bras, J. (2016). Production of cellulose nanofibrils: A review of recent advances. *Industrial Crops and Products, 93*, 2–25.

Nigmatullin, R., Johns, M. A., Muñoz-García, J. C., Gabrielli, V., Schmitt, J., Angulo, J., … Eichhorn, S. J. (2020). Hydrophobization of cellulose nanocrystals for aqueous colloidal suspensions and gels. *Biomacromolecules, 21*(5), 1812–1823.

Onyianta, A. J., Etale, A., Koev, T. T., Eloi, J.-C., Khimyak, Y. Z., & Stephen, J. E. (2022). Amphiphilic cellulose nanocrystals for aqueous processing of thermoplastics. *ACS Applied Polymer Materials, 4*(11), 8684–8693.

Pilathottathil, S., Kannan Kottummal, T., Thayyil, M. S., Mahadevan Perumal, P., & Ambichi Purakakath, J. (2018). Inorganic salt grafted ionic liquid gel electrolytes for efficient solid state supercapacitors: Electrochemical and dielectric studies. *Journal of Molecular Liquids, 264*, 72–79.

Plechkova, N. V., & Seddon, K. R. (2007). Ionic liquids: "Designer" solvents for green chemistry. In I. P. Tundo, A. Perosa, & F. Zecchini (Eds.), *Methods and reagents for green chemistry* (pp. 103–130). John Wiley & Sons, Inc.

Pringle, J. M., Golding, J., Baranyai, K., Forsyth, C. M., Deacon, G. B., Scott, J. L., & MacFarlane, D. R. (2003). The effect of anion fluorination in ionic liquids—Physical properties of a range of bis(methanesulfonyl)amide salts. *New Journal of Chemistry, 27*(10), 1504–1510.

Qu, P., Zhou, Y., Zhang, X., Yao, S., & Zhang, L. (2012). Surface modification of cellulose nanofibrils for poly(lactic acid) composite application. *Journal of Applied Polymer Science, 125*(4), 3084–3091.

Roman, M., & Winter, W. T. (2004). Effect of sulfate groups from sulfuric acid hydrolysis on the thermal degradation behavior of bacterial cellulose. *Biomacromolecules, 5*(5), 1671–1677.

Saito, T., Kuramae, R., Wohlert, J., Berglund, L. A., & Isogai, A. (2013). An ultrastrong nanofibrillar biomaterial: The strength of single cellulose nanofibrils revealed via sonication-induced fragmentation. *Biomacromolecules, 14*(1), 248–253.

Salam, A., Lucia, L. A., & Jameel, H. (2015). Fluorine-based surface decorated cellulose nanocrystals as potential hydrophobic and oleophobic materials. *Cellulose, 22*, 397–406.

Salem, K. S., Kasera, N. K., Rahman, M. A., Jameel, H., Habibi, Y., Eichhorn, S. J., … Lucia, L. A. (2023). Comparison and assessment of methods for cellulose crystallinity determination. *Chemical Society Reviews, 52*(18), 6417–6446.

Simon, J., Fliri, L., Drexler, F., Bacher, M., Sapkota, J., Ristolainen, M., Hummel, M., Potthast, A., & Rosenau, T. (2023). Debugging periodate oxidation of cellulose: Why following the common protocol of quenching excess periodate with glycol is a bad idea. *Carbohydrate Polymers, 310*, Article 120691.

Sonnier, R., Dumazert, L., Livi, S., Nguyen, T. K. L., Duchet-Rumeau, J., Vahabi, H., & Laheurte, P. (2016). Flame retardancy of phosphorus-containing ionic liquid based epoxy networks. *Polymer Degradation and Stability, 134*, 186–193.

Šturcová, A., Davies, G. R., & Eichhorn, S. J. (2005). Elastic modulus and stress-transfer properties of tunicate cellulose whiskers. *Biomacromolecules, 6*(2), 1055–1061.

Tang, C., Spinney, S., Shi, Z., Tang, J., Peng, B., Luo, J.-H., & Tam, K. C. (2018). Amphiphilic cellulose nanocrystals for enhanced pickering emulsion stabilization. *Langmuir : the ACS journal of surfaces and colloids, 34*(43), 12897–12905.

Ullah, Z., Bustam, M. A., Man, Z., Khan, A. S., Sarwono, A., Muhammad, N., … Haider, S. (2019). Phosphonium-based hydrophobic ionic liquids with fluorous anions for biodiesel production from waste cooking oil. *International journal of Environmental Science and Technology, 16*(3), 1269–1276.

Wang, X., Zhu, H., Girard, G. M. A., Yunis, R., MacFarlane, D. R., Mecerreyes, D., … Forsyth, M. (2017). Preparation and characterization of gel polymer electrolytes using poly(ionic liquids) and high lithium salt concentration ionic liquids. *Journal of Materials Chemistry A, 5*(45), 23844–23852.

Wang, Y., Wang, X., Xie, Y., & Zhang, K. (2018). Functional nanomaterials through esterification of cellulose: A review of chemistry and application. *Cellulose, 25*, 3703–3731.

Wasserscheid, P., & Welton, T. (2008). *Ionic liquids in synthesis*. Weinheim: Wiley-Vc.

Wei, Z., Sinko, R., Keten, S., & Luijten, E. (2018). Effect of surface modification on water adsorption and interfacial mechanics of cellulose nanocrystals. *ACS Applied Materials & Interfaces, 10*(9), 8349–8358.

Welton, T. (1999). Room-temperature ionic liquids. Solvents for synthesis and catalysis. *Chemical Reviews, 99*(8), 2071–2084.

Welton, T. (2011). Ionic liquids in green chemistry. *Green Chemistry, 13*(2), 225.

Wohlert, M., Benselfelt, T., Wågberg, L., Furó, I., Berglund, L. A., & Wohlert, J. (2022). Cellulose and the role of hydrogen bonds: Not in charge of everything. *Cellulose, 29*(1), 1–23.

Xu, F., Yu, J., Tesso, T., Dowell, F., & Wang, D. (2013). Qualitative and quantitative analysis of lignocellulosic biomass using infrared techniques: A mini-review. *Applied Energy, 104*, 801–809.

Xu, G., Nigmatullin, R., Koev, T. T., Khimyak, Y. Z., Bond, I. P., & Eichhorn, S. J. (2022). Octylamine-modified cellulose nanocrystal-enhanced stabilization of pickering emulsions for self-healing composite coatings. *ACS Applied Materials & Interfaces, 14*(10), 12722–12733.

Xu, G., Onyianta, A. J., Eloi, J.-C., Harniman, R. L., Laverock, J., Bond, I., … Eichhorn, S. J. (2024). Self-healing composite coating fabricated with a cystamine cross-linked cellulose nanocrystal-stabilized pickering emulsion. *Biomacromolecules, 25*(2), 715–728.

Yahia, M., Mei, S., Mathew, A. P., & Yuan, J. (2019). Linear main-chain 1,2,4-Triazolium poly(ionic liquid)s: Single-step synthesis and stabilization of cellulose nanocrystals. *ACS Macro Letters, 8*(10), 1372–1377.

Yue, C.-T., Sun, P., & Li, F.-W. (2022). Phosphonium ionic liquids. In S. Zhang (Ed.), *Encyclopedia of ionic liquids* (pp. 1004–1026). Singapore: Springer Nature Singapore.

Zhu, C., Koutsomitopoulou, A. F., Eichhorn, S. J., van Duijneveldt, J. S., Richardson, R. M., Nigmatullin, R., & Potter, K. D. (2018). High stiffness cellulose fibers from low molecular weight microcrystalline cellulose solutions using DMSO as co-solvent with ionic liquid. *Macromolecular Materials and Engineering, 303*(5), Article 1800029.

Zhu, C., Richardson, R. M., Potter, K. D., Koutsomitopoulou, A. F., van Duijneveldt, J. S., Vincent, S. R., … Rahatekar, S. S. (2016). High modulus regenerated cellulose fibers spun from a low molecular weight microcrystalline cellulose solution. *ACS Sustainable Chemistry & Engineering, 4*(9), 4545–4553.